Naval Research Laboratory
Washington, DC 20375-5320

NRL/MR/6770--94-7609

Transport Efficiency Studies for Light-Ion Inertial Confinement Fusion

D. V. Rose

JAYCOR, Inc.
Vienna, VA

P. F. Ottinger

Pulsed Power Physics Branch
Plasma Physics Division

C. L. Olson

Sandia National Laboratories
Albuquerque, NM

September 30, 1994

REPORT DOCUMENTATION PAGE

Form Approved OMB No. 0704-0188

1. AGENCY USE ONLY (*Leave Blank*)	2. REPORT DATE	3. REPORT TYPE AND DATES COVERED
	September 30, 1994	Interim

4. TITLE AND SUBTITLE

Transport Efficiency Studies for Light-Ion Inertial Confinement Fusion

5. FUNDING NUMBERS

67-0879-0-2

6. AUTHOR(S)

D.V. Rose,[1] P.F. Ottinger, and C.L. Olson[2]

7. PERFORMING ORGANIZATION NAME(S) AND ADDRESS(ES)

Naval Research Laboratory
Washington, DC 20375-5320

8. PERFORMING ORGANIZATION REPORT NUMBER

NRL/MR/6770--94-7609

9. SPONSORING/MONITORING AGENCY NAME(S) AND ADDRESS(ES)

Sandia National Laboratories
Albuquerque, NM 87185

10. SPONSORING/MONITORING AGENCY REPORT NUMBER

SNL FAO AI-7233
DOE DE-AC04-94AL8500

11. SUPPLEMENTARY NOTES

[1]JAYCOR, Inc., Vienna, VA 22182
[2]Sandia National Laboratories, Albuquerque, NM 87185

12a. DISTRIBUTION/AVAILABILITY STATEMENT

Approved for public release; distribution unlimited.

12b. DISTRIBUTION CODE

13. ABSTRACT (*Maximum 200 words*)

The proposed Laboratory Microfusion Facility (LMF) will require ≥10 MJ of 30 MeV lithium ions to be transported and focused onto high-gain, high-yield inertial confinement fusion targets. The light-ion LMF approach used a multimodular system with individual ion extraction diodes as beam sources. Several transport schemes are being considered to deliver the individual ion beams to the centrally located target. Previous work [P.F. Ottinger, D.V. Rose, and C.L. Olson, J. Appl. Phys. 75, 4402 (1994)] examined the effect of time-of-flight bunching on energy transport efficiency, η_t, under realistic constraints on diode operation, beam transport, and packing. Target design considerations suggest that the instantaneous power efficiency, Γ_t, be maximized near peak power. Because of time-of-flight bunching, peak power occurs at the end of the power pulse for LMF designs. This work examines the effect of power efficiency tuning on η_t for three transport schemes. Results indicate that tuning the power pulse to maximize Γ_t, at about three-quarters through the pulse provides high power efficiency at the end of the pulse while still maintaining high η_t. In addition to power efficiency tuning, effects on η_t from variations of the diode impedance model and the diode voltage waveform are also examined.

14. SUBJECT TERMS

Light-ion
Inertial confinement fusion

15. NUMBER OF PAGES

51

16. PRICE CODE

17. SECURITY CLASSIFICATION OF REPORT	18. SECURITY CLASSIFICATION OF THIS PAGE	19. SECURITY CLASSIFICATION OF ABSTRACT	20. LIMITATION OF ABSTRACT
UNCLASSIFIED	UNCLASSIFIED	UNCLASSIFIED	UL

NSN 7540-01-280-5500

Standard Form 298 (Rev. 2-89)
Prescribed by ANSI Std 239-18
298-102

CONTENTS

TRANSPORT EFFICIENCY STUDIES FOR LIGHT-ION INERTIAL CONFINEMENT FUSION

I. Introduction

The Laboratory Microfusion Facility (LMF) has been proposed for the study of high-gain, high-yield inertial confinement fusion (ICF) targets.[1] A multimodular light-ion approach, based on Hermes-III technology, is under investigation.[1,2] This approach requires the transport and focusing of a number of intense ion beams over distances of several meters to a centrally located, high-gain, high-yield ICF target. The distance between the target and beam generators provides for packing of the beam generators around a target chamber of > 100 cm radius, and isolation of the diode hardware from the explosion. In addition, the transport distance allows for time-of-flight (TOF) bunching of the beams to achieve power multiplication. Several beam transport and focusing schemes are being evaluated for LMF,[3,4] including ballistic transport with solenoidal lens focusing (BTSF),[5] and ballistic focusing with z-discharge transport (ZDT),[6] or wire-guided transport (WGT).[7] The baseline approach for LMF utilizes the BTSF scheme with a ballistic transport distance L (diode to lens) of 250 cm and a focal distance F (lens to target) of 150 cm. The LMF system is schematically illustrated for BTSF in Fig. 1. The alternate transport schemes, ZDT and WGT are shown in Figs. 2 and 3, respectively. In both of these transport schemes, the beam is ballistically focused over a distance F of 150 cm onto the transport channel entrance and transported a distance L of 250 cm to the target. In addition to these three transport schemes, self-pinched transport has been proposed for transporting intense ion beams for LMF.[8] Since the BTSF, ZDT, and WGT schemes have been the most extensively studied to date, self-pinched transport will not be discussed in this work. However, results for self-pinched transport should be similar to those of ZDT.

Manuscript approved August 15, 1994.

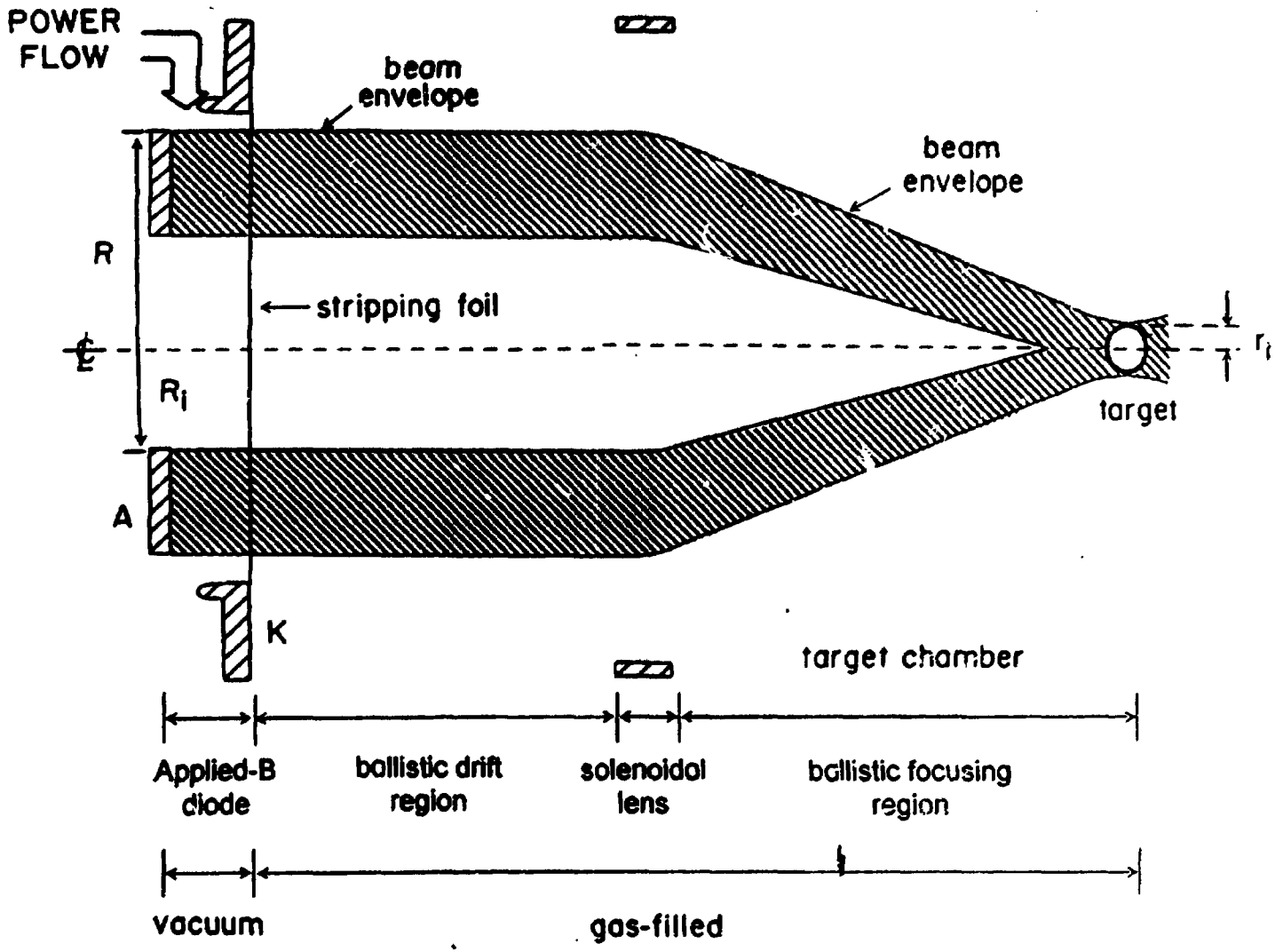

Fig. 1 - Schematic of BTSF system.

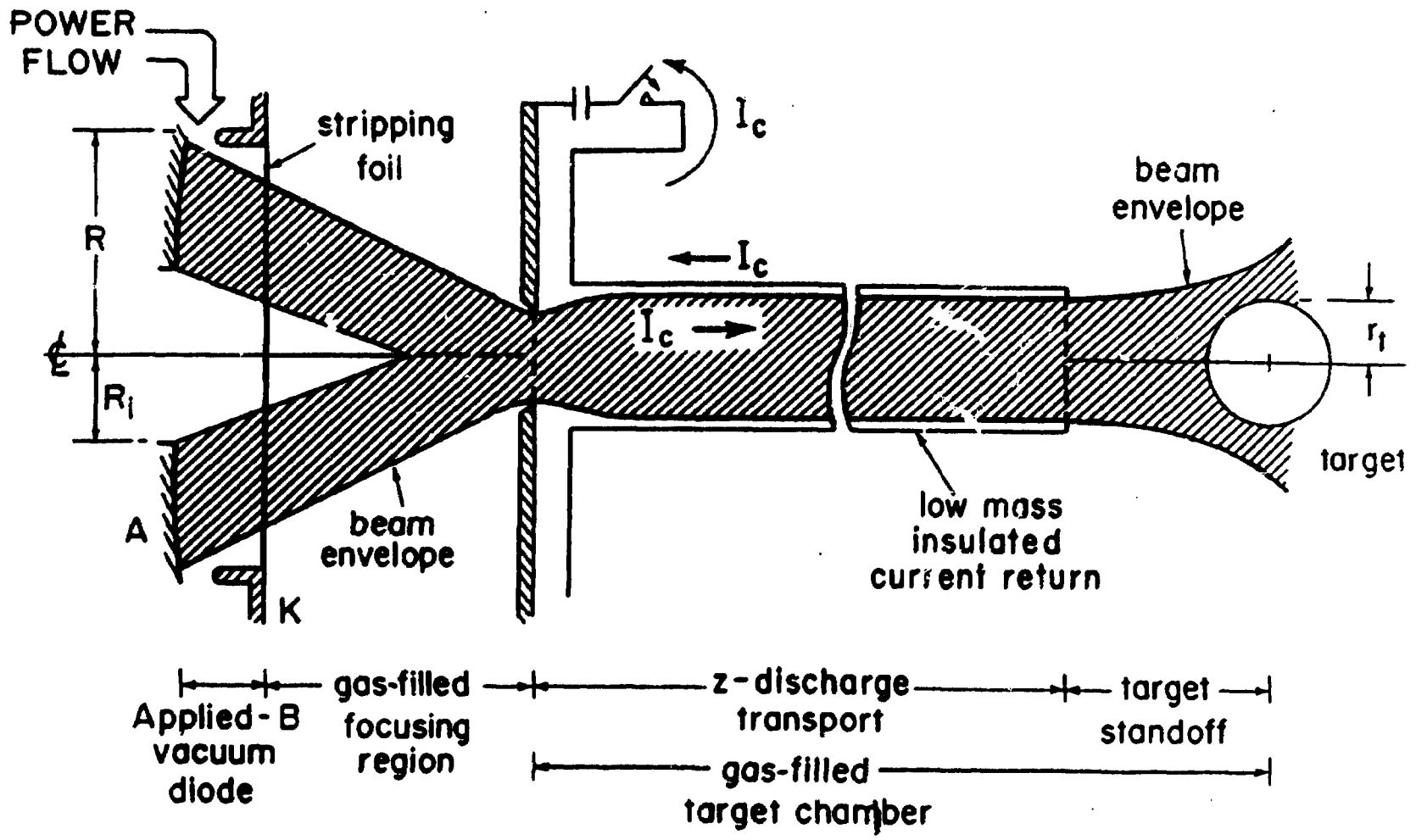

Fig. 2 - Schematic of ZDT system.

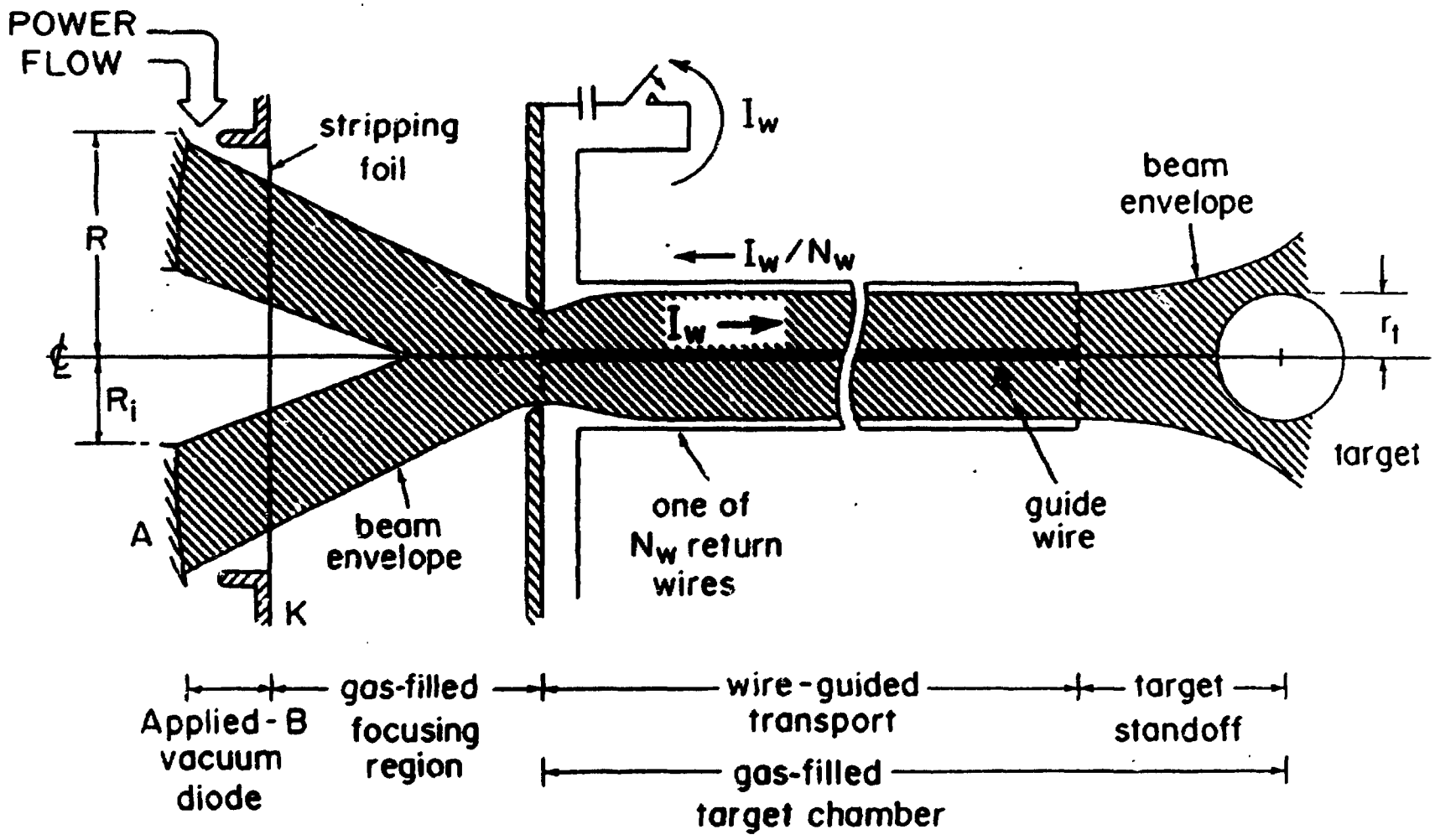

Fig. 3 - Schematic of WGT system.

A previous analysis[9] examined the effect of time-of-flight bunching on energy transport efficiency, η_t , under realistic constraints on diode operation, beam transport, and packing. The energy transport efficiency η_t is defined here as the ratio of total ion energy delivered to the target to the total ion energy produced in the diodes. This effort extends the previous analysis to examine the impact of systematic variations in several key model parameters. These parameters include tuning the peak power coupling between the beam and the target, current scaling for the diode impedance model, and diode voltage variations about the ideal voltage ramp for TOF bunching. The square microdivergence profile for the ion source model, used in the previous analysis, has also been replaced with a Gaussian microdivergence profile.

Power efficiency Γ_t is defined as the ratio of the instantaneous transported ion power on target to the power at that same instant of an ideal bunched beam pulse at the target location as defined by the product of current and voltage will be given in Eqs. (15) and (16). Because of chromatic focusing effects, Γ_t changes in time as the voltage changes. Typically, the achromatic matching condition (for BTSF) or the ballistic focal length (for ZDT and WGT) are fixed at mid-pulse to optimize η_t. In this case Γ_t peaks near mid-pulse. However, Γ_t can be tuned to peak at other times at the expense of lower η_t. Previous work[9] examined chromatic effects on η_t with power efficiency tuned to peak at mid-pulse. Target design considerations indicate that peak power should be delivered at the end of the pulse.[10] In this paper, the time of peak power efficiency is varied between the mid-point and the end of the voltage pulse to determine the effect on η_t. Results indicate that tuning the power pulse to maximize Γ_t at about three-quarters through the pulse provides high power efficiency at the end of the pulse while still maintaining high η_t. For BTSF, this yields 89 % instantaneous power efficiency at the tail of the pulse with η_t of 73 % for parameters of interest (L = 250 cm, F = 150 cm, a diode radius of 15 cm, and a microdivergence of 5 mrad) for a system with 20 modules and 20 MJ of ion energy available at the diodes.

Section II of this paper reviews the ion source model used in this work and highlights changes from the previous analysis. The effect on η_i due to modifying the microdivergence profile for all three transport schemes is also examined in this section. In Sec. III, the effect of power efficiency tuning on η_i is examined. Section IV of this paper examines the impact on η_i due to variations in the diode impedance model and the diode voltage waveform. This paper is summarized in Sec. V. Note that when comparing two efficiency numbers, absolute differences (in %) are quoted rather than percentage changes.

II. Ion Source Model

The ion source model is based on the extraction applied-B diode with an annular emitting surface extending from outer radius R to inner radius $R_i = R/2$. Ions accelerated across the vacuum gap, Δ, in the diode are bent toward the axis by the self-magnetic field of the beam. For small angles, this bending angle $\Theta_b(r,t)$ is $\omega_c\Delta/v$, where $v(t)$ is the ion speed, and ω_c is the beam ion cyclotron frequency associated with the self-magnetic field in the diode region so that $\omega_c = 2eZ_d I_d / rm_i c^2$. Here, $I_d(t)$ is the ion current in the diode, eZ_d and m_i are the beam ion charge in the diode and the ion mass, and c is the speed of light. Uniform current density is assumed in the annular emitting region of the diode.

A stripping foil separates the diode vacuum region from the gas-filled transport region. Singly charged lithium ions accelerated across the vacuum gap are stripped to Li^{+3} as they enter the gas-filled region. For applied-B extraction diodes, the position and shape of this stripping foil are determined by ion beam angular momentum considerations. This topic is addressed in detail in Ref. 9. For the purposes of this work, the width of the vacuum gap, Δ, in the BTSF case is determined solely from the achromatic matching condition[5] and it will be assumed that both achromatic and angular

momentum conditions have been satisfied.[9] For ZDT and WGT, it is assumed that Δ is fixed at 4 cm, independent of radius.

As illustrated in Figs. 4 and 5, ions are assumed to leave the diode region distributed in a cone of half-angle Θ_μ about a steering angle $\Theta_s = \Theta_b(r,t) + \Theta_a(r)$, where Θ_μ is the source microdivergence, and $\Theta_a(r)$ is due to the anode surface shape (assuming no anode plasma motion). Unlike the previous analysis[9], Θ_μ is assumed to have a Gaussian profile in velocity space and is independent of radius and time. The impact of this change is discussed at the end of this section. Figure 4 shows the beam extracted parallel to the axis for BTSF and Fig. 5 shows a focused extraction of the beam appropriate for ZDT and WGT. Since Θ_b varies as $V_d^{(k-1/2)}$, where $V_d(t)$ is the diode accelerating voltage, and diode current scales as V^k (typically k is assumed to be 2.0), Θ_a can compensate for Θ_b at only one point in time. At this time, referred to as the tuning time, the instantaneous power transport efficiency is optimized. The previous analysis used a tuning time near mid-pulse, when the average voltage V_o is reached, optimizing η_t. For this analysis, the tuning time, expressed in terms of the tuned diode voltage V_{tune}, is varied between the middle and the end of the pulse in order to study the impact of changing the time of optimal power efficiency (delivered to the target) on η_t.

The ideal ramped voltage and current pulses produced by the diode are

$$V_d(t) = \frac{V_d(0)}{\left(1 - \frac{t}{T}\frac{\alpha - 1}{\alpha}\right)^2}, \qquad (1)$$

and

$$I_d(t) = I_{do}\left(\frac{V_d(t)}{V_o}\right)^k, \qquad (2)$$

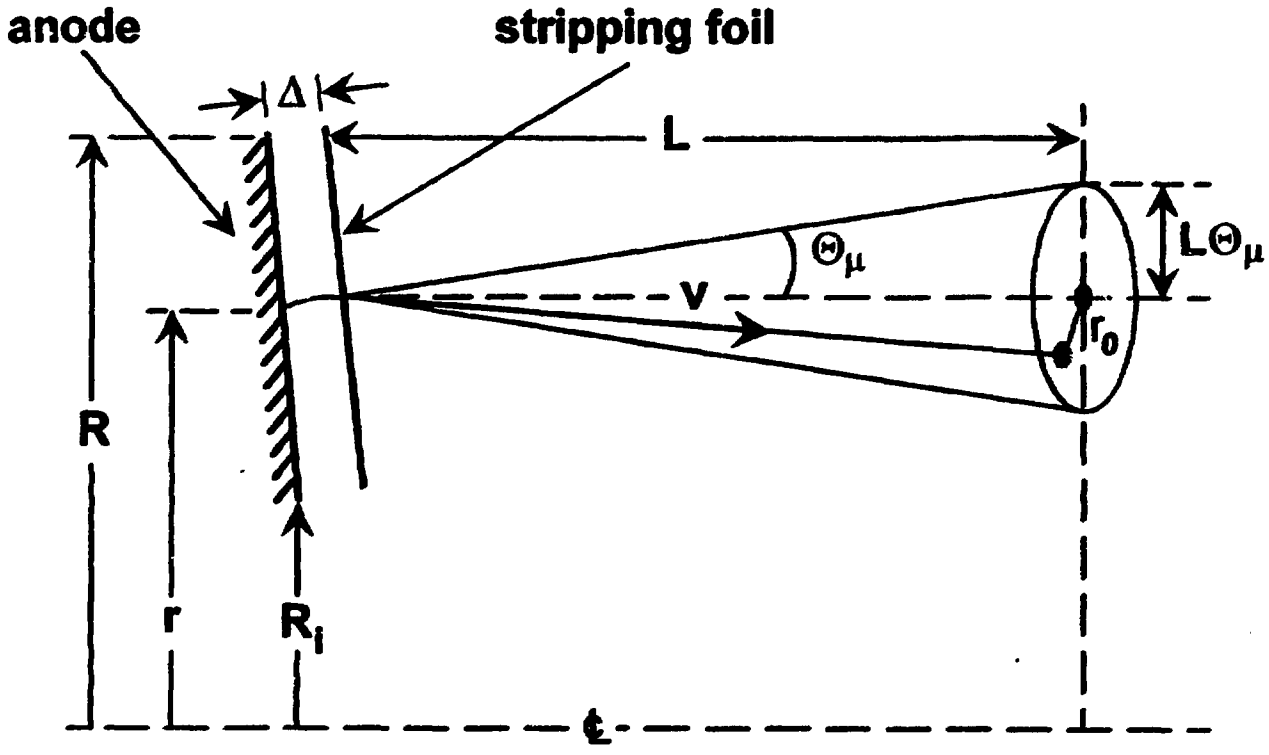

Fig. 4 - Injection geometry for BTSF.

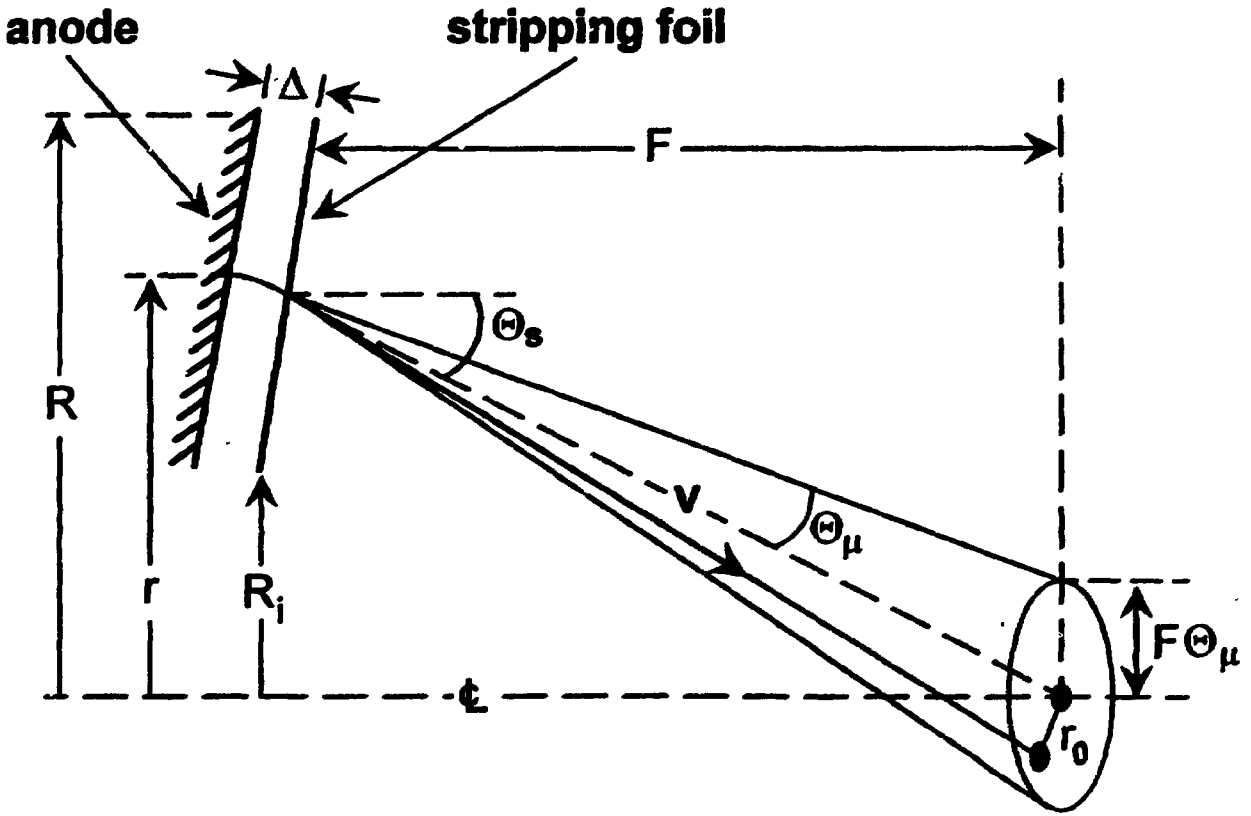

Fig. 5 - Injection geometry for ZDT and WGT.

where T is the arrival time of the beam front at the target, $V_d(0)$ is the initial voltage at time $t = 0$, and α is the bunching factor. The average value of the voltage, V_o, is defined as $\left(V_d(\tau_d)+V_d(0)\right)/2$, where τ_d is the initial pulse length and I_{do} is the diode ion current when $V_d(t) = V_o$. A power pulse given by Eqs. (1) and (2) will time-of-flight compress to a pulse length of $\tau_b = \tau_d / \alpha$ at a time T after the start of the pulse.

The total path length for the beam from the diode to the target is $D = v_d(0)T$, where $v_d(0) = (2eZ_dV_d(0)/m_i)^{1/2}$, for a non-relativistic beam. Evaluating Eq. (1) at $t = \tau_d$ and substituting the resulting expression for $V_d(\tau_d)$ into the definition of V_o yields

$$V_d(0) = 2V_o - V_d(\tau_d) = \frac{2V_o\xi^2}{(1+\xi^2)}\,, \tag{3}$$

where

$$\xi = 1-\left(\frac{\tau_d}{T}\right)\left(\frac{\alpha-1}{\alpha}\right). \tag{4}$$

Equation (3) relates $V_d(0)$ and $V_d(\tau_d)$ for given values of $\xi(\alpha, \tau_d, T)$. Substituting Eq. (3) into the definition of D yields

$$T^2 = \frac{m_iD^2}{4eZ_dV_o}\left(\frac{1+\xi^2}{\xi^2}\right), \tag{5}$$

which is a transcendental equation for T in terms of given values for m_i, D, V_o, and $\xi(\alpha,\tau_d,T)$. Using Eq. (2) for $I_d(t)$ and setting the total beam energy per module,

$$E_d = \int_0^{\tau_d} I_d(t)V_d(t)dt = \frac{I_{do}}{V_o^k}\int_0^{\tau_d}\left(V_d(t)\right)^{k+1}dt\,, \tag{6}$$

equal to E_s/N specifies I_{do} for given values of V_o , E_s , N, k, and $\xi(\alpha, \tau_d, T)$. The system energy, E_s, is the total ion energy available from the N diodes and is related to the energy on target, E_t, by $E_t = \eta_t E_s$. Substituting for $V_d(t)$ from Eq. (1) into Eq. (6) and performing the integration yields

$$I_{do} = \frac{(2k+1)E_s}{2^{k+1}NV_o\tau_d}\left(\frac{1-\xi}{\xi}\right)\frac{\left(1+\xi^2\right)^{k+1}}{\left(1-\xi^{2k+1}\right)}, \tag{7}$$

where ξ is given in Eq. (4).

Using the assumption of uniform current density in the annular diode and the impedance model given in Eq. (2), Θ_b can be written as

$$\Theta_b(r,t) = -\Theta_o\left(\frac{V_d(t)}{V_o}\right)^{k-1/2}\left(\frac{r}{R}-\frac{R}{4r}\right), \tag{8}$$

where

$$\Theta_o = \frac{8I_{do}\Delta}{3c^2R}\left(\frac{eZ_d}{2m_iV_o}\right)^{1/2}. \tag{9}$$

Since Θ_a is assumed fixed in time, Eq. (8) will lead to an inward sweeping of Θ_s over the duration of the pulse.

At the tuning time, $t(V_{tune})$, the steering angle is set equal to $-r/F$, so that the beam is ballistically focused a distance F from the diode for ZDT and WGT. For BTSF, F is set equal to ∞, so that the beam is extracted parallel to the axis. Combining this condition on the steering angle with Θ_b yields the appropriate anode shape

$$\Theta_a(r) = -\frac{r}{F}+\Theta_o\left(\frac{V_{tune}}{V_o}\right)^{k-1/2}\left(\frac{r}{R}-\frac{R}{4r}\right). \tag{10}$$

The beam ion steering angle defined previously[9], is now modified to include the voltage tuning parameter, V_{tune}, by combining Eqs. (8) and (10), yielding

$$\Theta_s(r,t) = -\frac{r}{F} + \Theta_o\left(\frac{V_{tune}}{V_o}\right)^{k-\frac{1}{2}}\left(1-\left(\frac{V_d(t)}{V_{tune}}\right)^{k-\frac{1}{2}}\right)\left(\frac{r}{R}-\frac{R}{4r}\right). \qquad (11)$$

This equation combines both geometric anode shaping as well as bending due to self-magnetic field focusing of the beam in the vacuum region of the diode. This form of Eq. (11) is appropriate for ZDT and WGT. For BTSF, where the beam is extracted parallel to the transport symmetry axis (i.e., $F = \infty$) at the time the voltage rises to V_{tune}, the term $-r/F$ in Eq. (11) is set to zero.

For BTSF, the diode and solenoidal lens can be treated as an achromatic lens pair for a particular value of r, assuming small variations about the tuning voltage, V_{tune}. The focal length of the solenoid at the tuning voltage is given by[5]

$$F_{tune} = \frac{4v_{tune}^2}{\omega_c^2 L_s}, \qquad (12)$$

where L_s is the axial length of the solenoid, and v_{tune} is the ion velocity associated with the tuning voltage V_{tune}. The lens pair is matched for $r = R$, which maximizes the number of ions chromatically focused because the diode is assumed to have uniform current density. Following the analysis performed in Ref. 9, the matching condition becomes

$$\Theta_o = \frac{4R}{3F_{tune}(k-1/2)}\left(\frac{V_o}{V_{tune}}\right)^{k-1/2}, \qquad (13)$$

where Θ_o is given by Eq. (9), resulting in the following expression for Δ.

$$\Delta = \frac{c^2 R^2}{2(k-1/2) I_{do} F_{tune}} \left(\frac{V_o}{V_{tune}} \right)^{k-1/2} \left(\frac{2 m_i V_o}{e Z_d} \right)^{1/2}, \qquad (14)$$

where I_{do} is given in Eq. (7).

The source microdivergence for all cases considered in Sec. III and IV of this paper assumes a Gaussian profile, with the half-width, half-maximum, Θ_μ, selected to be 5 mrad. Previous calculations[5,6,9] assumed a square microdivergence profile with a half-width of Θ_μ. Therefore, additional losses in the "wings" (for $\Theta > \Theta_\mu$) are expected, resulting in a reduction in η_t. Since about 25 % of the ions reside in the wings, additional losses could be significant. A comparison of square and Gaussian profiles for each transport scheme is given in Figs. 6-8. For these calculations, $N = 20$ modules, $E_s = 20$ MJ, $\alpha = 2$, $\Theta_\mu = 5$ mrad, $k = 2$, and $V_{tune} = V_o$. Focus sweep effects[9] (because $\alpha > 1$) and system design constraints[5,6,7] will be the predominate mechanisms governing η_t for these results. The BTSF scheme, with Δ matched according to Eq. (14), is shown in Fig. 6. For the cases shown, η_t is reduced by 12 % or less. The potential reduction in η_t due to the use of a Gaussian microdivergence profile is minimized in the BTSF case, because the spot size $F\Theta_\mu$ is smaller than the target radius. For $F = 150$ cm and $\Theta_\mu = 5$ mrad, a spot size of 0.75 cm is obtained while a target radius of 1 cm is used. This situation does not apply to the ZDT (Fig. 7) and WGT (Fig. 8) schemes because the beam is apertured down at the entrance of the transport channel to the spot size $F\Theta_\mu$. For these cases, η_t is reduced by at most 9 % and 20 % for ZDT and WGT respectively. The greater overall reduction in η_t for WGT as seen in Fig. 8 is a result of the Gaussian distributed profile being forward peaked. More low-angular-momentum ions strike the guide wire and are removed from the beam.

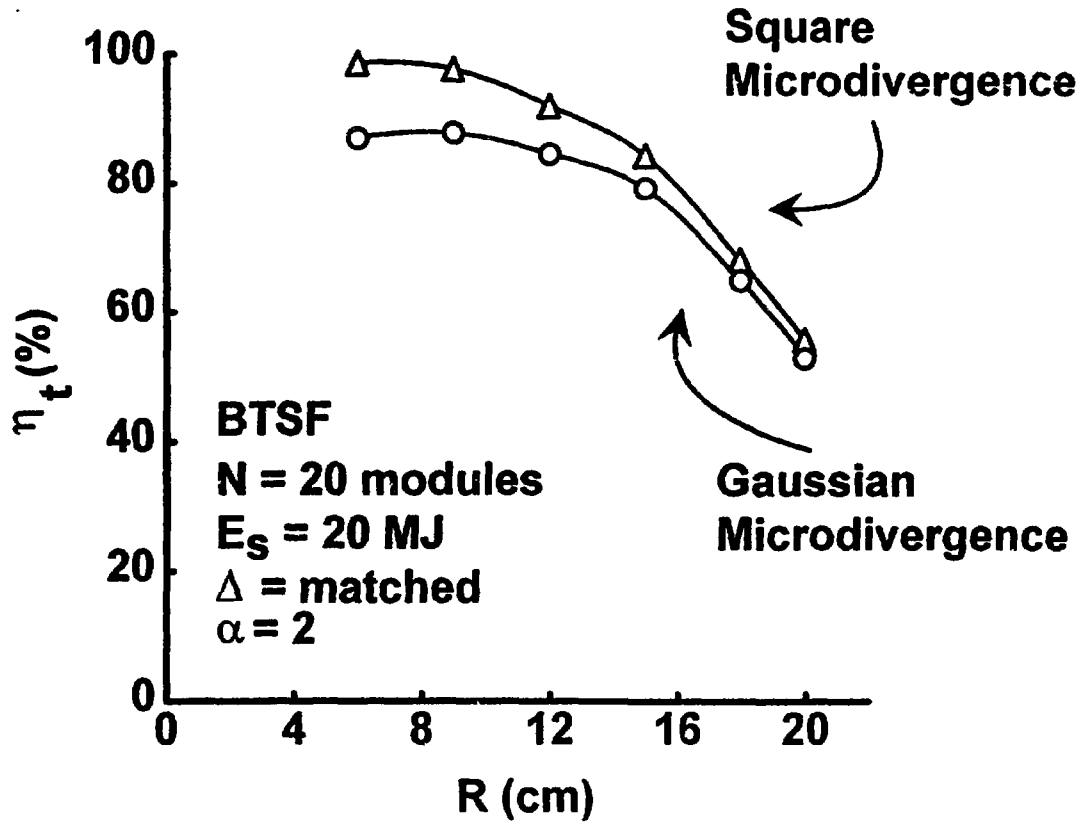

Fig. 6 - Plot of η_t vs. R with $\alpha = 2$ for BTSF, comparing square (uniform) and Gaussian microdivergence profiles with $\Theta_\mu = 5$ mrad.

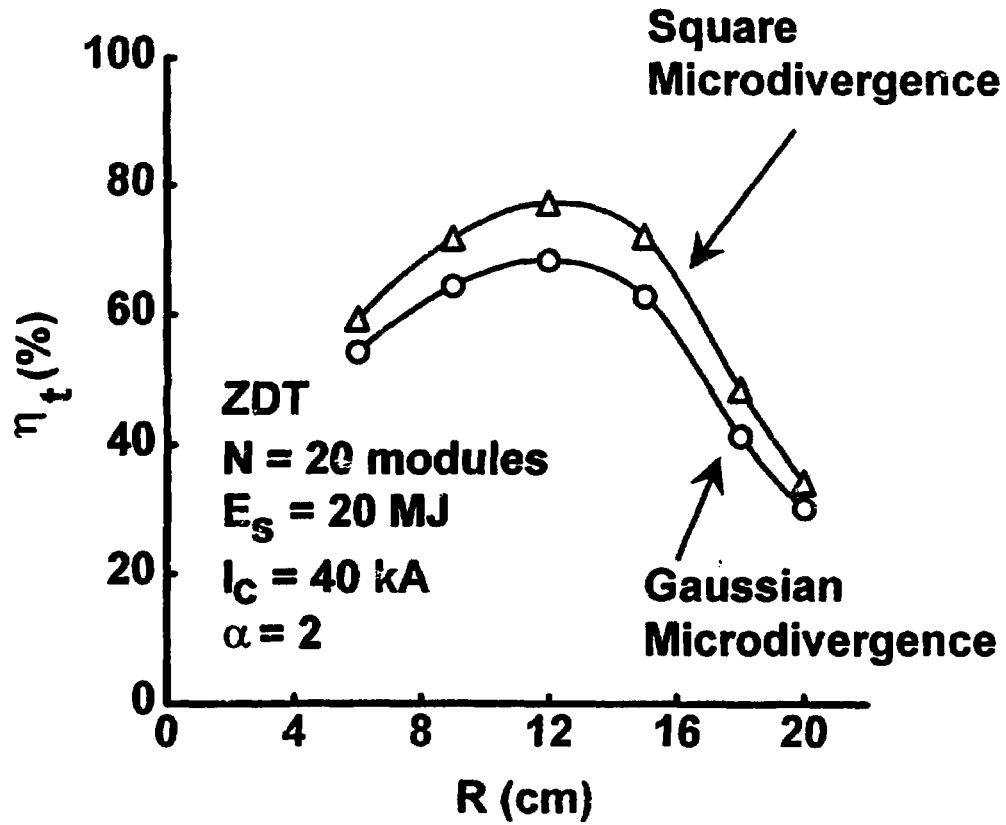

Fig. 7 - Plot of η_t vs. R with $\alpha = 2$ for ZDT, comparing square (uniform) and Gaussian microdivergence profiles with $\Theta_\mu = 5$ mrad.

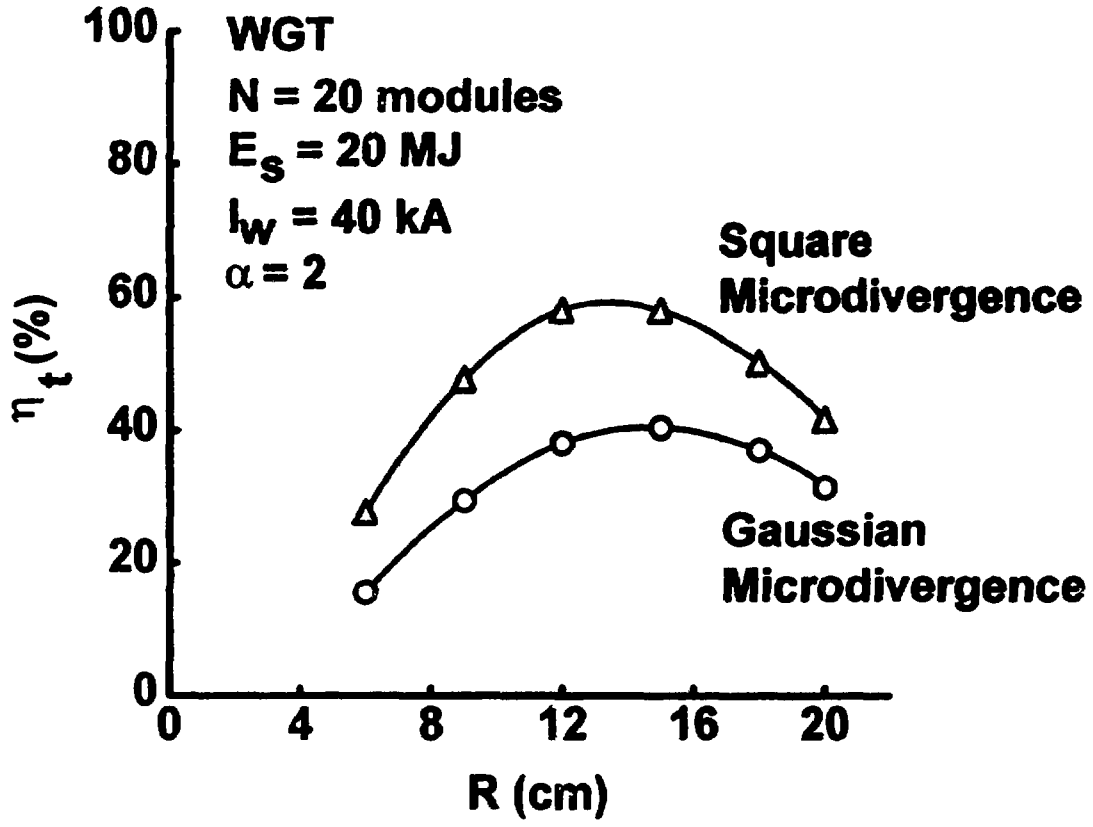

Fig. 8 - Plot of η_t vs. R with $\alpha = 2$ for WGT, comparing square (uniform) and Gaussian microdivergence profiles with $\Theta_\mu = 5$ mrad.

For the calculations presented here, it is assumed that Li^{+1} ions are accelerated in the diode and are stripped to Li^{+3} as they pass through the foil. A previous analysis[9] considered a range of values for E_s, N, and α. For this work, these values will be fixed at E_s = 20 MJ, N = 20, and α = 2. In addition, it will be assumed that V_o = 30 MV, D = 400 cm, and τ_b = 15 ns (so that τ_d = 30 ns). In addition, R will be varied for some calculations between 6 and 20 cm, with R = 15 cm used as the baseline diode radius. A centrally located, spherical target of radius r_t = 1 cm is assumed at $z = D$ from each of the N diodes.

III. Power Efficiency Tuning

ICF target design considerations indicate that peak power delivered to the target should occur at the end of the driver pulse.[10] This can be accomplished by tuning the voltage for peak power efficiency near the end of the pulse. However, as V_{tune} increases from V_o toward $V(\tau_d)$, η_t decreases. This section examines the impact on η_t of tuning, or moving, the time of peak power later in the pulse.

Allowing the voltage and current waveforms, Eqs. (1) and (2), to evolve in time as the beam is projected ballistically to the target plane at $z = D$, yields

$$V_t(t) = \frac{V_t(T)}{\left(\alpha - t\dfrac{\alpha - 1}{T}\right)^2}, \tag{15}$$

and

$$I_t(t) = \alpha I_{to}\left(\frac{Z_t V_t(t)}{Z_d V_o}\right)^k, \tag{16}$$

for $T \le t \le T + \tau_b$. Here $V_t(T) = Z_d V_d(0) / Z_t$ and $I_{to} = Z_t I_{do} / Z_d$ account for the stripping of the beam from Li^{+1} to Li^{+3} in the diode region, before the beam is transported. Equations (15) and (16) ignore path differences in the transverse components of the beam due to microdivergence, focusing, scattering, stopping, etc. and assume 100% transport efficiency. The product of Eqs. (15) and (16) gives the ideal power on target as a function of time. The ratio of the instantaneous power on target to the ideal instantaneous power is Γ_t.

The time at which the voltage pulse rises to the effective voltage $Z_d V_{tune} / Z_t$ at the target (due to stripping of the beam) is $t_t(V_{tune}) = T + t_d(V_{tune}) / \alpha$ or

$$t_t(V_{tune}) = \frac{T}{\alpha - 1}\left(\alpha - \sqrt{\frac{V_d(0)}{V_{tune}}}\right), \qquad (17)$$

where $t_d(V_{tune})$ is the time the voltage in the diode rises to V_{tune} which can be obtained from Eq. (1).

For this study, three different voltage tunings were considered at one-half, three-quarters, and the end of the pulse. The voltages corresponding to these tuning times (in the diode) are denoted as $V_{1/2}$, $V_{3/4}$, and $V_{4/4}$, and are given as 29.743 MV, 31.401 MV, and 33.201 MV, respectively for $\alpha = 2$, $k = 2$, $V_o = 30$ MV, $T = 148$ ns, $E_s = 20$ MJ, and $N = 20$ modules. It should be noted that $V_o \neq V_{1/2}$ because the average value of Eq. (1) over the pulse length τ_d does not occur at $\tau_d/2$. Simulations calculating the instantaneous power efficiency at the tuning time, Γ_t^{tune}, the instantaneous power efficiency at the end of the pulse, Γ_t^{end}, and the total transported energy efficiency, η_t, were carried for the BTSF, ZDT, and WGT schemes. A three-dimensional, non-relativistic orbit code was used with 20,000 test particles to give adequate statistics. Full charge and current neutralization is assumed. For the BTSF scheme, the ATHETA code,[11] was used to

generate the solenoidal lens magnetic field maps used in the orbit code. For these simulations, a Gaussian microdivergence profile was used with Θ_μ = 5 mrad.

The impact on η_t of changing the tuning time is qualitatively illustrated for BTSF in Fig. 9 for R = 15 cm, k = 2, and α = 2. This set of plots shows the radius of beam particles arriving at the target position, z = 400 cm, as a function of time for three different tunings. About 5 % of the total number of particles used in a typical simulation is represented in these plots. Since each simulation particle is equally weighted in current (but not potential), the increase in power at the tail of the pulse is partially illustrated in Fig. 9 by an increase in the number of particles per time interval. Particles at or below the dashed line at $r = r_t$ = 1 cm determine η_t. It is immediately evident that as $t_t(V_{tune})$ is selected to be later in the pulse, more particles do not strike the target, lowering η_t.

For the BTSF scheme, foil placement to achieve achromatic matching is satisfied at only one time in the pulse (the tuning time) and is governed by Eq. (14). For each of the simulations illustrated in Figs. 10-12, different magnetic fields strengths had to be employed in order to optimally focus the ions of velocity v_{tune} onto the target. Figure 10 plots Γ_t^{tune} at the three different tuning voltages. The fall off in Γ_t^{tune} for $R > 15$ cm is due primarily to the packing constraint which limits the maximum solenoidal lens radius. This issue is discussed in detail in Ref. 9. It is evident that the same Γ_t^{tune} can be achieved regardless of which of the three tuning voltages is selected. However, in Fig. 11, the instantaneous power efficiency at the end of the pulse, Γ_t^{end}, does depend on the tuning voltage chosen. Tuning the voltage to the middle of the pulse results in a reduction in Γ_t^{end} by 10 % on average for R = 9 to 18 cm compared with tuning the voltage to the end of the pulse. Conversely, the total energy transported to the target for the $V_{4/4}$ case relative to the $V_{1/2}$ case is reduced by an average of 17 % for R = 9 to 18 cm as illustrated in Fig. 12. It is evident from this that for BTSF, selecting a tuning time at three-quarters of the pulse length leads to only a slight loss in η_t while maintaining near-optimal power in the tail of the pulse. For the baseline case of R = 15 cm, a drop of 6 %

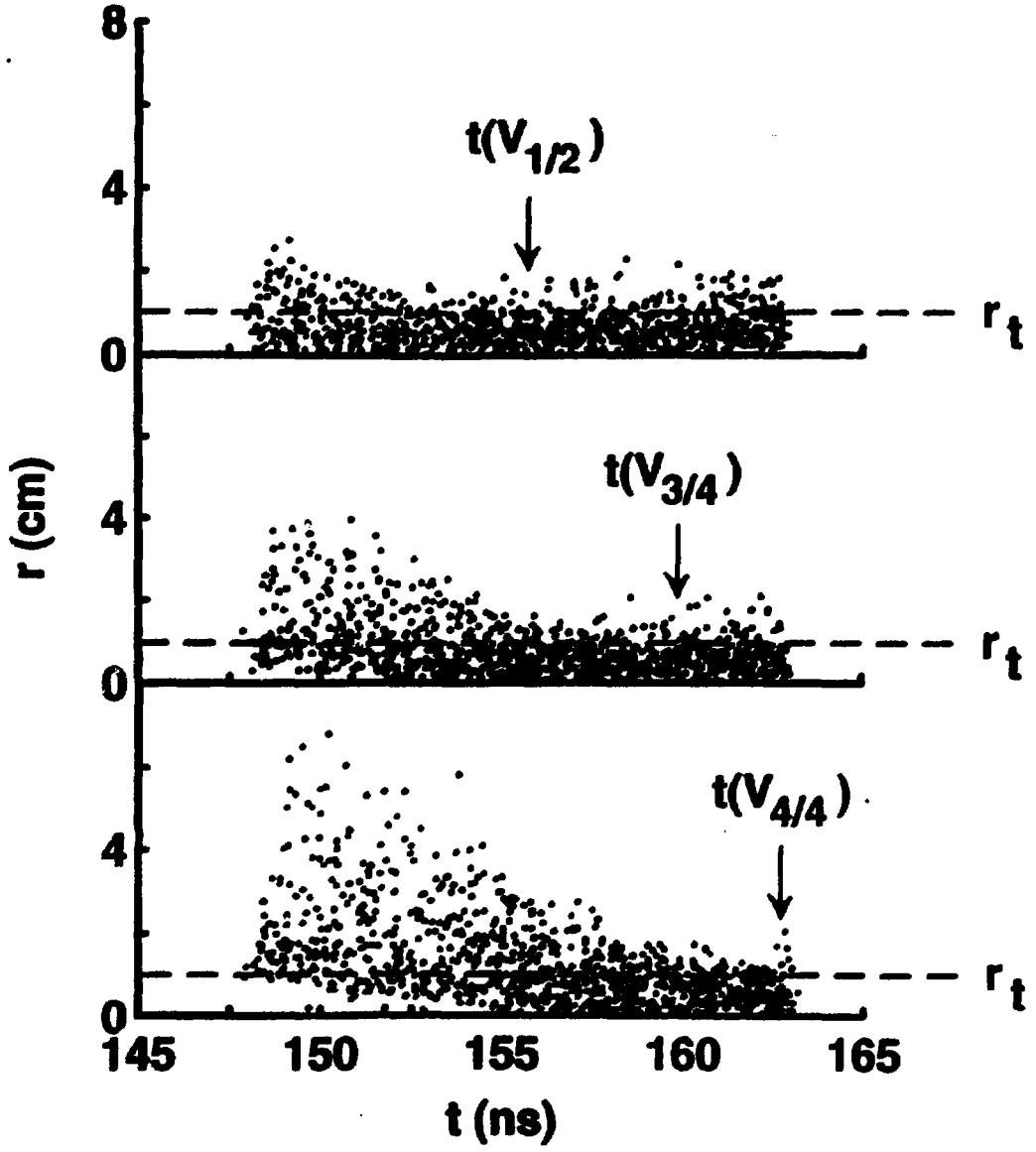

Fig. 9 - Plot of beam particle radius, r, vs. t at the target plane, z = 400 cm. Three different tuning times are plotted, $t(V_{1/2})$, $t(V_{3/4})$, and $t(V_{4/4})$. In each plot, 5 % of the total number of particles used in the simulation are represented. For these calculations, R = 15 cm, k = 2, α = 2, N = 20, E_s = 20 MJ, and Θ_μ = 5 mrad.

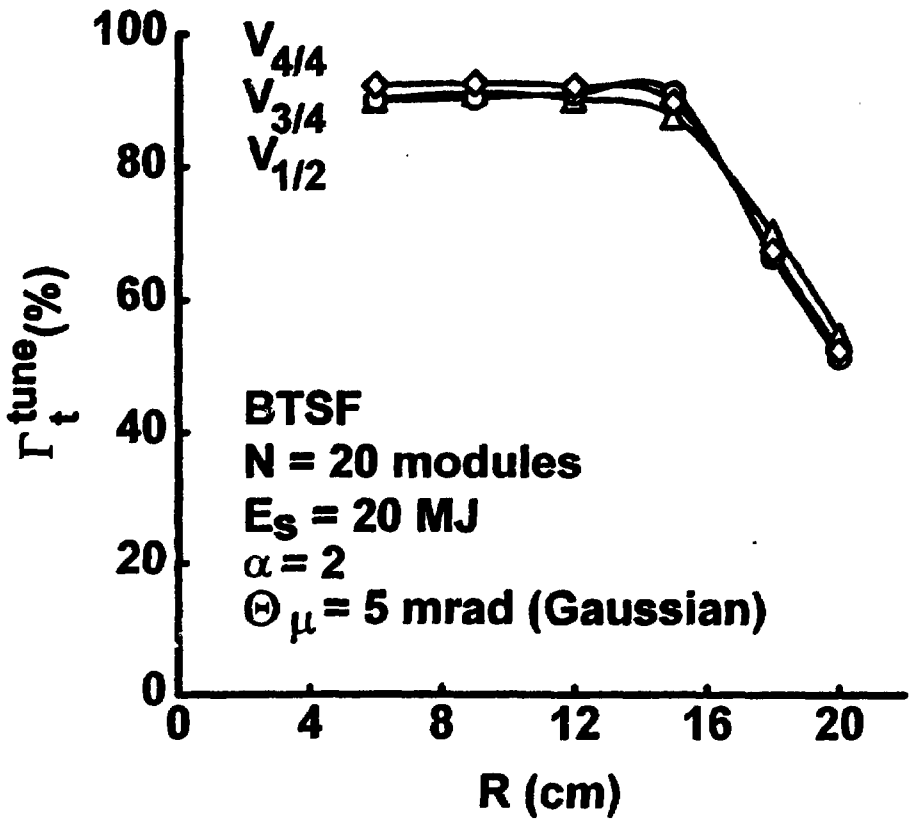

Fig. 10- Plot of Γ_t^{tune} vs. R for BTSF. The individual curves are for voltage tunings of $V_{1/2}$, $V_{3/4}$, and $V_{4/4}$.

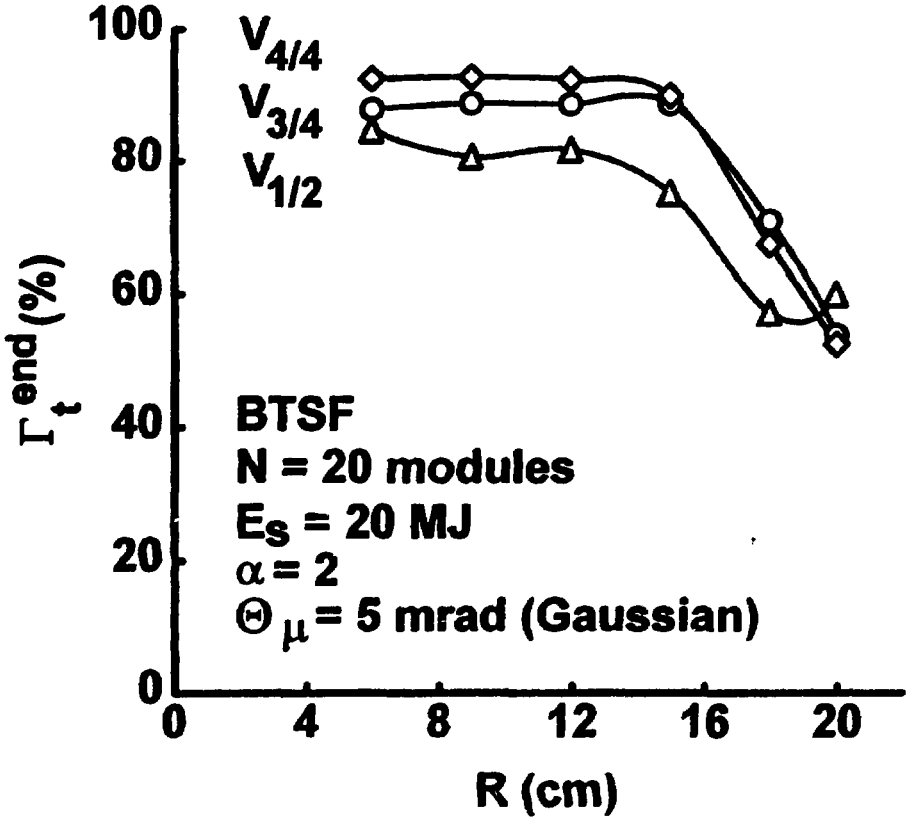

Fig. 11 - Plot of Γ_t^{end} vs. R for BTSF. The individual curves are for voltage tunings of $V_{1/2}$, $V_{3/4}$, and $V_{4/4}$.

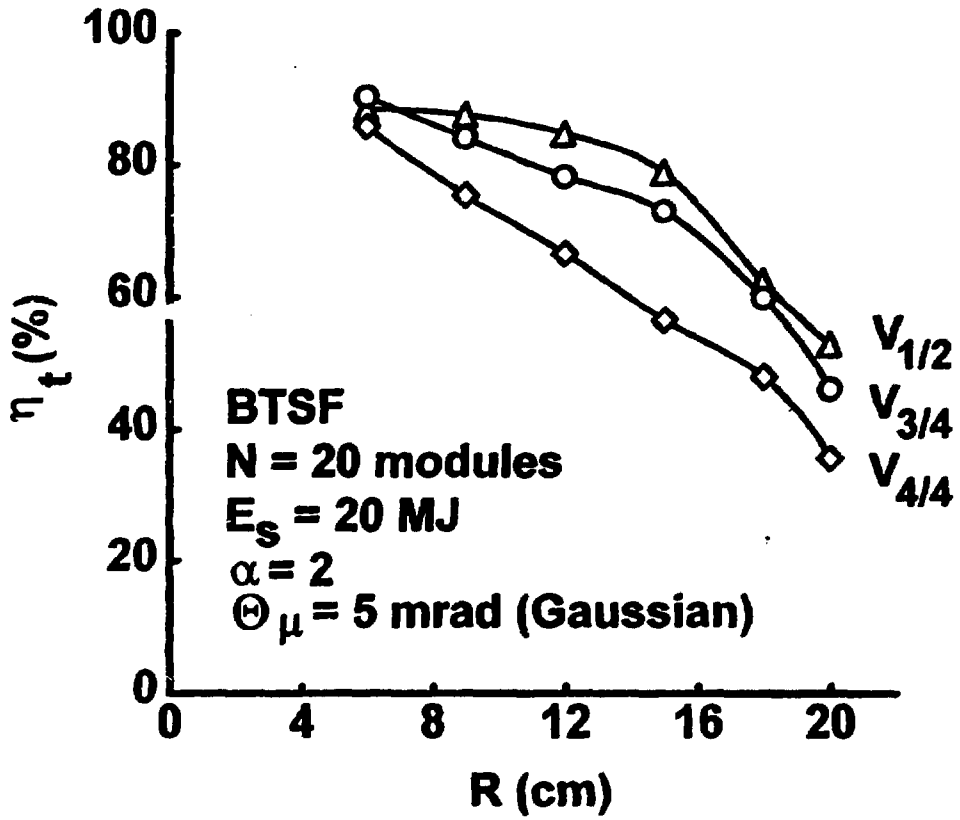

Fig. 12- Plot of η_t vs. R for BTSF. The individual curves are for voltage tunings of $V_{1/2}$, $V_{3/4}$, and $V_{4/4}$.

in η_t results in a 14 % gain in Γ_t^{end} when shifting the tuning from the middle to three-quarters through the pulse. For this baseline case with $V_{3/4}$ tuning, η_t = 73 % and Γ_t^{end} = 89 %. The maximum Γ_t^{end} is 90 % which occurs for the $V_{4/4}$ tuning.

For ZDT, Δ is held constant at 4 cm. A discharge channel current, I_c, of 40 kA with a channel wall radius of 1 cm was chosen, which confines the entire beam for $\alpha = 1$ and $R \leq 10.5$ cm.[6] For R greater than 10.5 cm, ions are lost to the channel wall. Due to packing constraints, the discharge channels must terminate at a standoff distance[6] from the target given by $d = r_t(N/2)^{1/2}$. For this study, d = 3.16 cm and the length of the transport channel is then $D - F - d$ which is on the order of 250 cm. An aperture of inner radius $F\Theta_\mu$ = 0.75 cm is located at the entrance to the discharge system at F.

As found in the BTSF case, simulations for ZDT indicate that Γ_t^{tune} does not change as the tuning time is moved from the middle to the end of the pulse, as shown in Fig. 13. However, Fig. 14 shows that the focus sweep effect dramatically reduces the power in the tail of the pulse for the mid-pulse tuning time for R = 6 to 15 cm. For this same range in R, the average drop in η_t that results from moving the tuning from the middle to the end of the pulse is 14 %. Figure 15 illustrates that over the entire range of R, that tuning to the three-quarters time in the pulse results in an almost negligible loss in η_t. In particular, at R = 15 cm, η_t was found to be 62 % for both $V_{1/2}$ and $V_{3/4}$. Also Γ_t^{end} gained 12 % to a value of 62 % out of a maximum value of Γ_t^{end} = 69 % for the R = 15 cm case.

For WGT, a wire current, I_w, of 40 kA was chosen. A wire radius, r_w, of 0.035 cm was used throughout and is determined to be the minimum radius required to avoid melting.[7] Return current wires are placed at radius of about 1.4 times the average beam radius in order to minimize losses due to chaotic orbit effects while maintaining as compact a WGT system as possible for packing.[7] The standoff distance is about 2.5 times that of the ZDT system,[9] with a transport distance $D - F - d$ which is on the order of

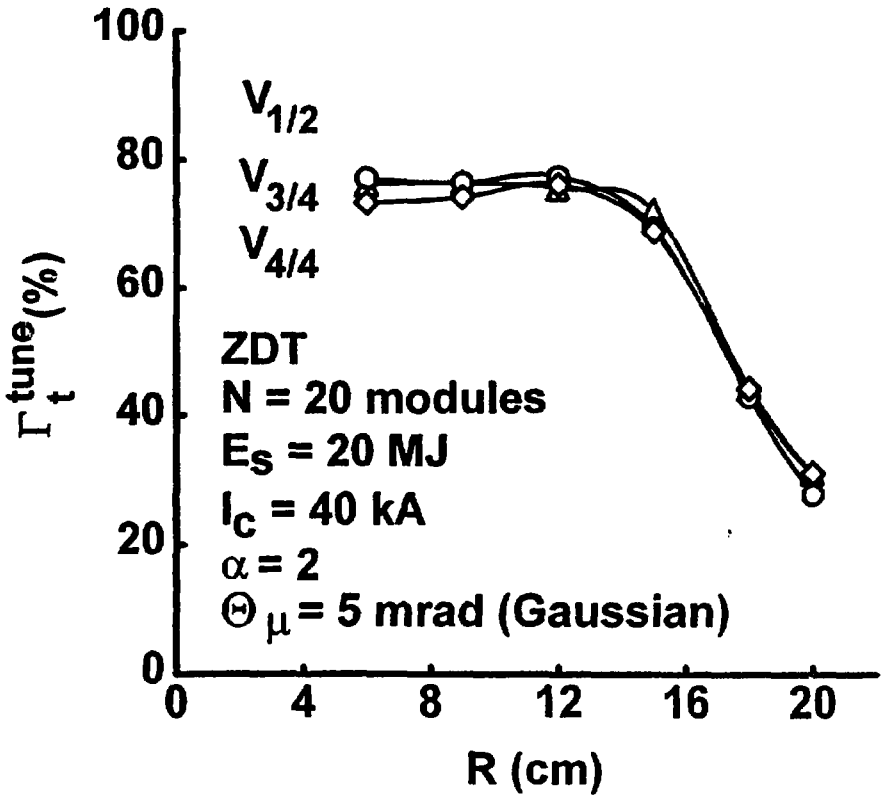

Fig. 13- Plot of Γ_t^{tune} vs. R for ZDT. The individual curves are for voltage tunings of $V_{1/2}$, $V_{3/4}$, and $V_{4/4}$.

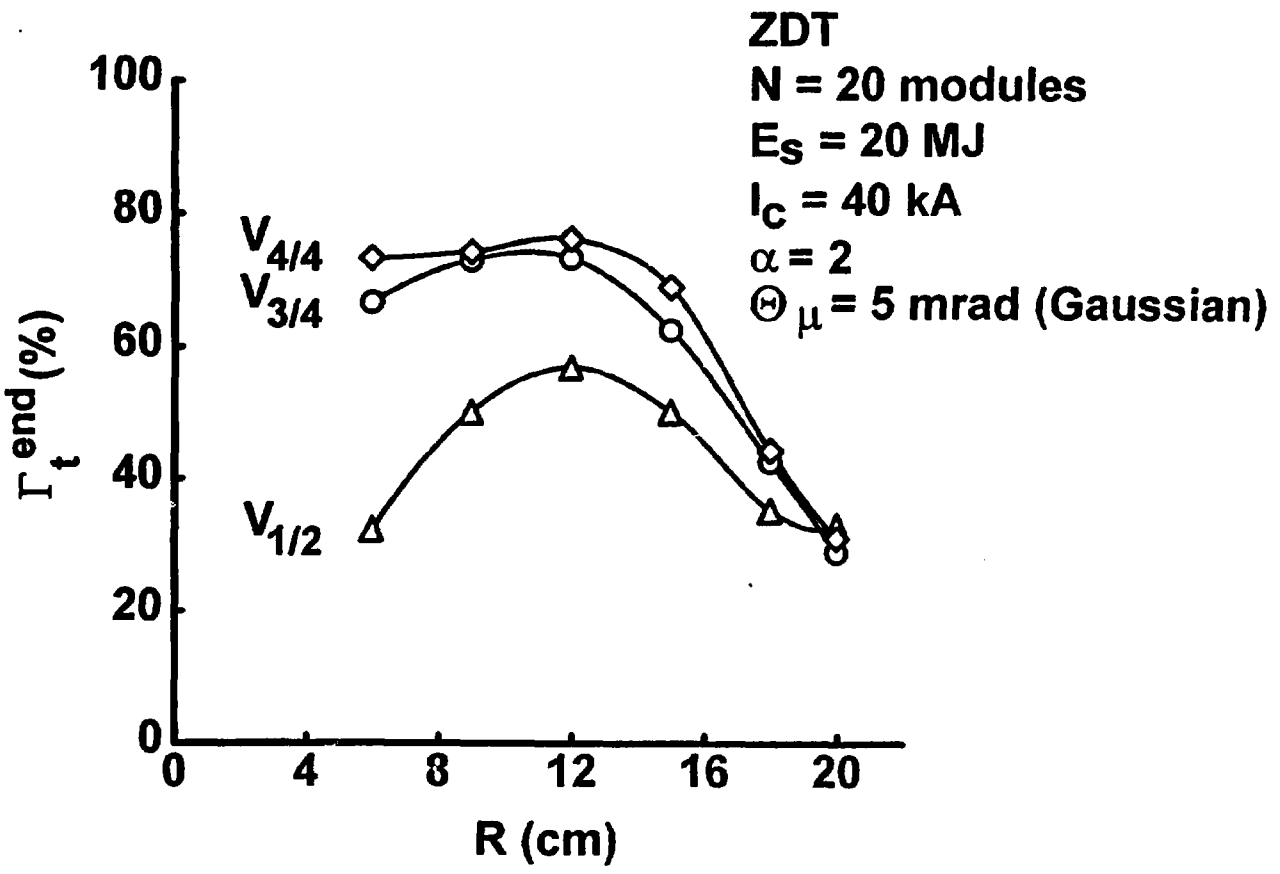

Fig. 14- Plot of Γ_t^{end} vs. R for ZDT. The individual curves are for voltage tunings of $V_{1/2}$, $V_{3/4}$, and $V_{4/4}$.

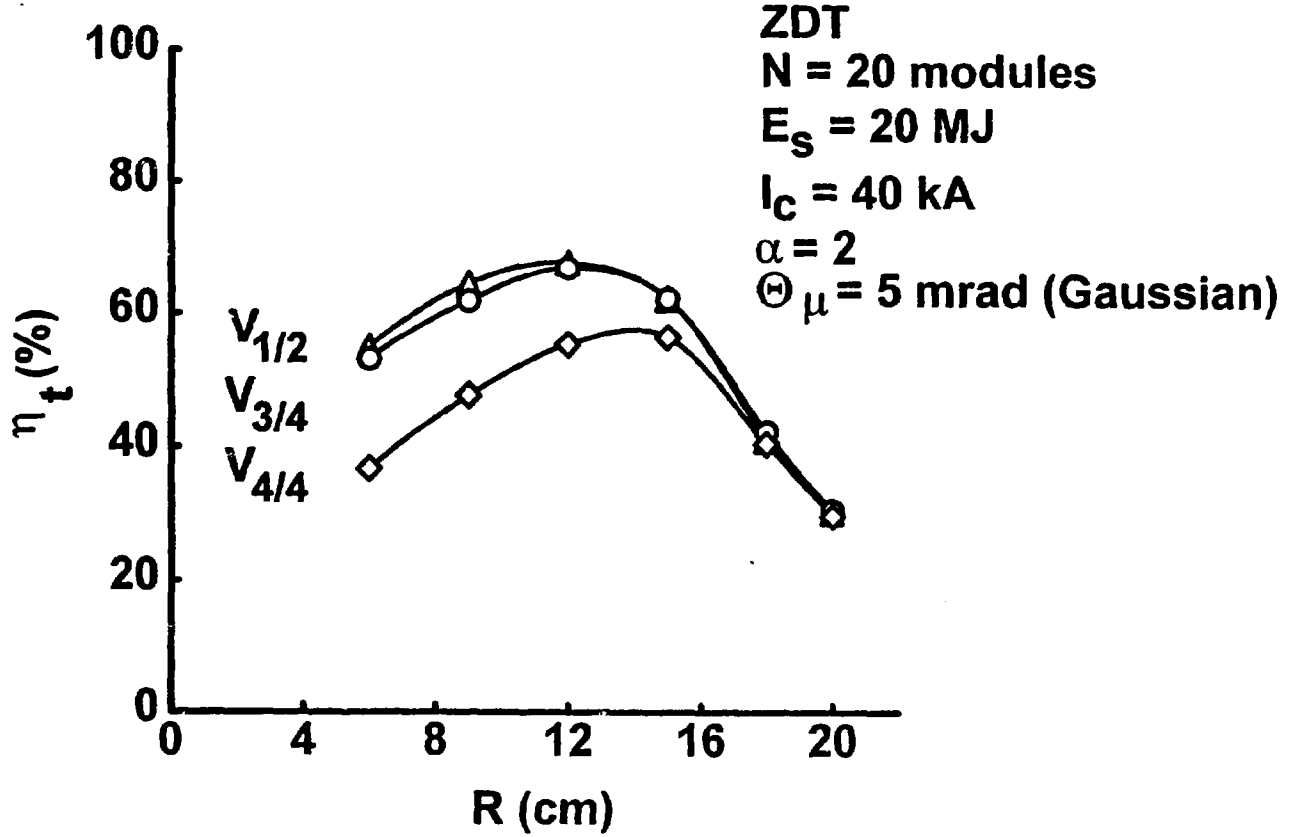

Fig. 15 - Plot of η_t vs. R for ZDT. The individual curves are for voltage tunings of $V_{1/2}$, $V_{3/4}$, and $V_{4/4}$.

250 cm. An aperture of radius $F\Theta_\mu$ = 0.75 cm is located at the entrance to the wire system at F.

As for BTSF and ZDT, simulations for WGT indicate that Γ_t^{tune} does not change as the tuning time is moved from the middle to the end of the pulse, as shown in Fig. 16. In Fig. 17, moving the tuning from the end to the middle of the pulse results in an average drop of 13 % in Γ_t^{end} over the range R = 6 to 20 cm. As for the BTSF and ZDT, moving the tuning time from mid-pulse to three-quarters of the pulse length results in only a small average drop in Γ_t^{end} from peak values (about 4 % for tuning at $V_{3/4}$ rather than $V_{4/4}$). In Fig. 18, this choice results in virtually no change in η_t. The optimum case occurs for R = 15 cm where η_t = 40 %, and Γ_t^{end} = 43 % for $V_{3/4}$ tuning. The maximum Γ_t^{end} of 47 % occurs when R = 15 cm with $V_{4/4}$ tuning.

IV. Impedance Model Variations and Non-Ideal Accelerator Wave Forms

The design of the LMF applied-B diode for use in a light-ion LMF system is currently being investigated. One possible design employs a two-stage[12] scheme, whose particular benefits include high beam purity, lower beam microdivergence, control of impedance behavior, reduced accelerating voltage per stage, and commensurately smaller insulating magnetic fields. Since the actual impedance model of such a diode is currently under evaluation, it is desirable to consider the impact of the diode impedance model on the efficiency results presented in Section II. This is achieved by changing the values of k in Eq. (2) over a range of values that seem possible for a two-stage diode design. Figure 19 illustrates the dramatic change in Δ over k in the range 0.75 to 2.5, according to Eq. (14), with $V_{tune} = V_o$, and R = 15 cm. Note that Δ scales as R^2, so that for R = 10 cm, Δ increases from 3 cm to 12 cm as k decreases from 2.5 to 1.0. The actual placement of individual foils to relax the requirements on Δ is discussed elsewhere[9,12] and is beyond the scope of this work.

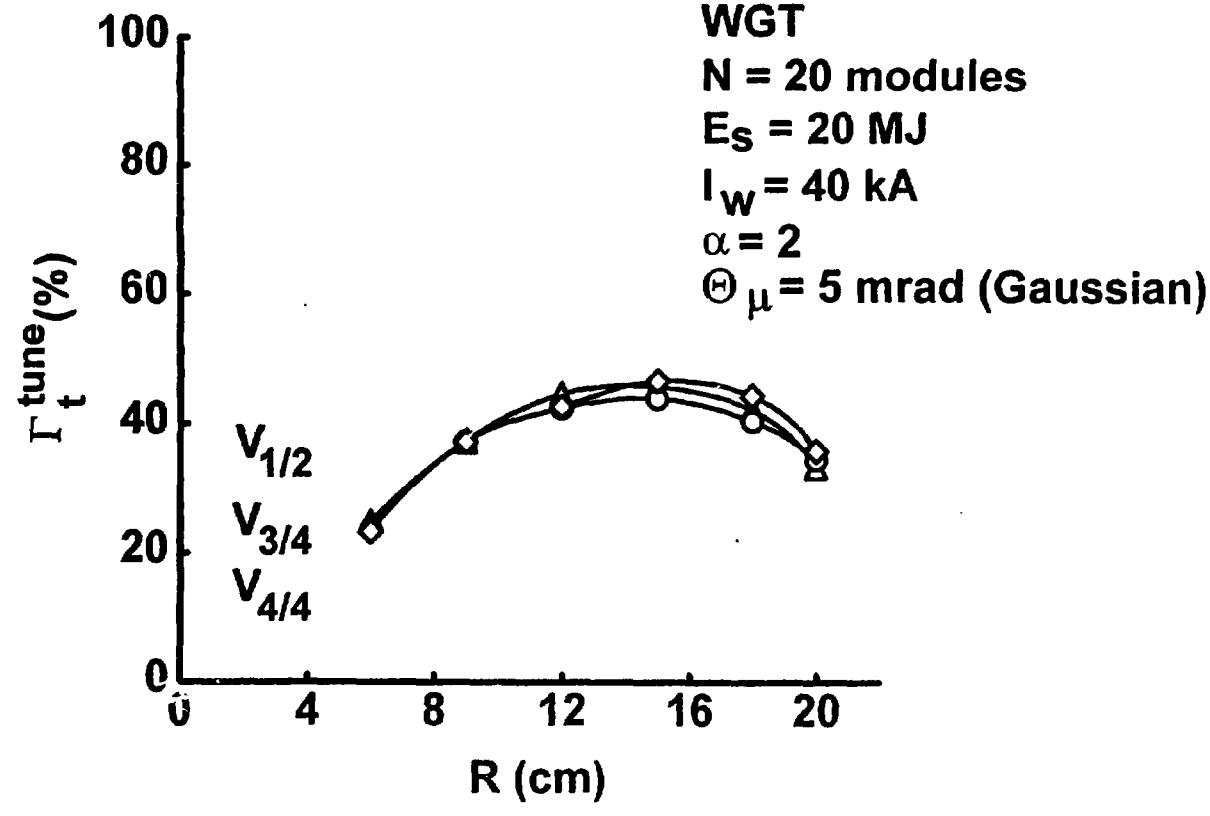

Fig. 16- Plot of Γ_t^{tune} vs. R for WGT. The individual curves are for voltage tunings of $V_{1/2}$, $V_{3/4}$, and $V_{4/4}$

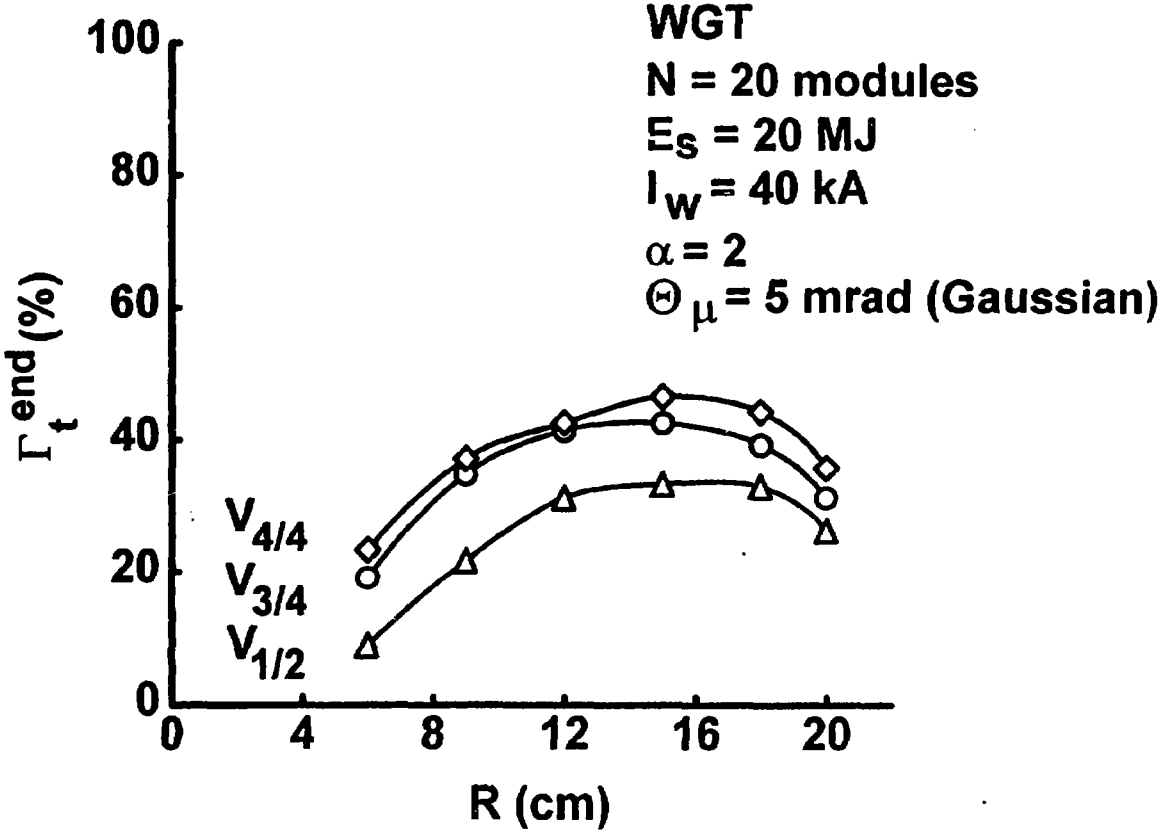

Fig. 17- Plot of Γ_t^{end} vs. R for WGT. The individual curves are for voltage tunings of $V_{1/2}$, $V_{3/4}$, and $V_{4/4}$.

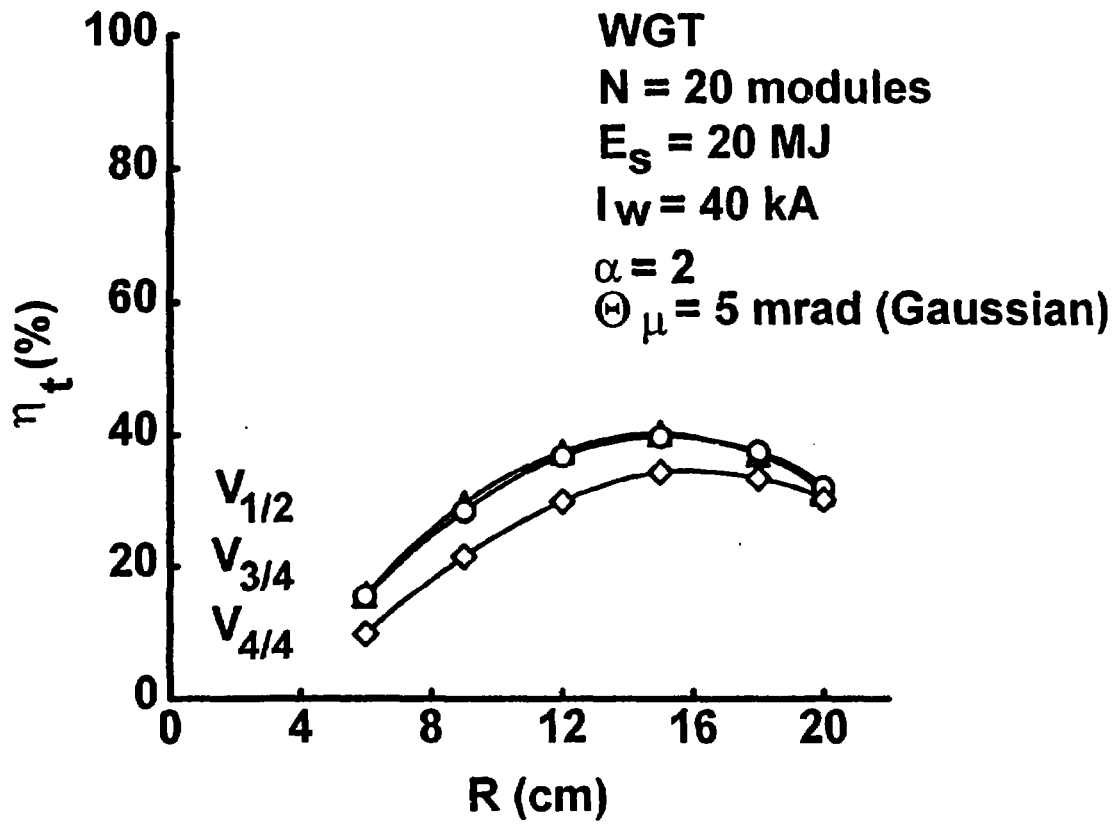

Fig. 18- Plot of η_t vs. R for WGT. The individual curves are for voltage tunings of $V_{1/2}$, $V_{3/4}$, and $V_{4/4}$.

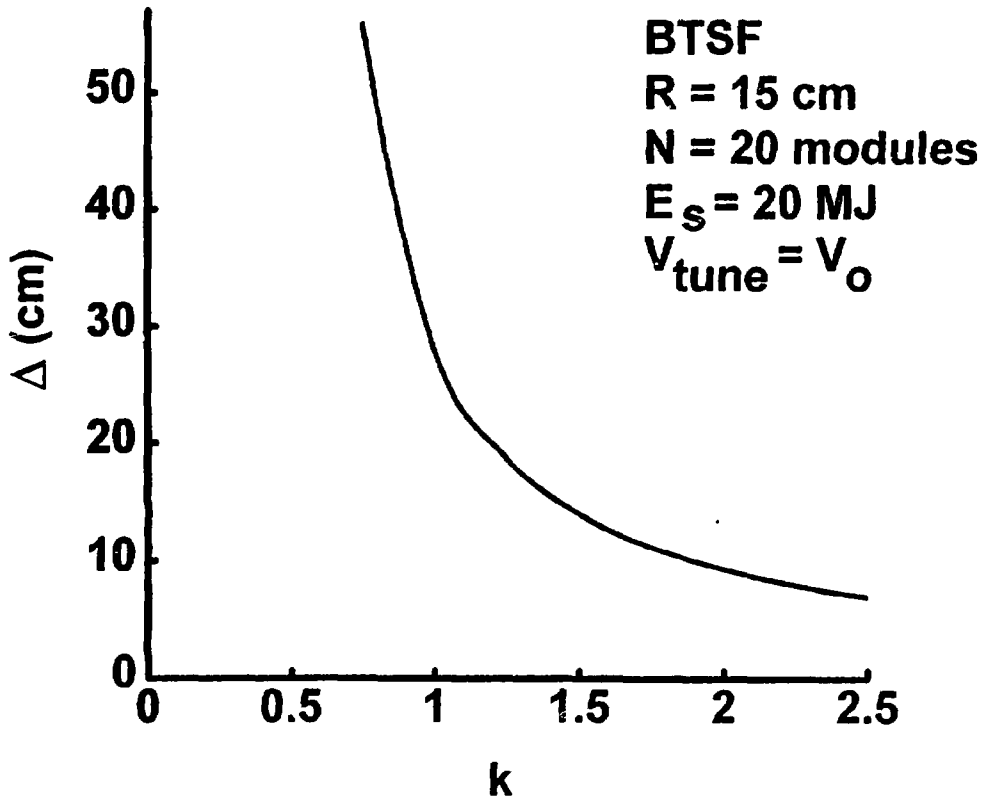

Fig. 19- Plot of Δ vs. *k* for BTSF matched case.

In Fig. 20, the impact of varying k over the range 0.75 to 2.5 is shown for BTSF, ZDT, and WGT with R = 15 cm, Θ_μ = 5 mrad, α = 2, $V_{tune} = V_o$ = 30 MV, and F_{tune} = 150 cm. For BTSF, virtually no effect of varying k is observed within the range 0.75 and 2.5, indicating that the enhanced focus-sweep effect resulting from larger values of k has little effect on η_f for this nearly achromatic system. The effect of the target size exceeding the spot size contributes to this stability of η_f. For ZDT and WGT, η_f linearly decreases with increasing k for a variation of 11 % and 8 %, respectively over the range of k considered. Therefore, it can be anticipated that the potential benefits of two-stage diodes can be exploited without a significant change in the results presented in Sec. II and III. Since k will most likely decrease for a two-stage diode, η_f would improve slightly for ZDT and WGT.

Another issue of concern to the design of a light-ion ICF system is deviation of the power pulse from the ideal waveform given by the product of Eqs. (1) and (2). Ramped voltage waveforms produced by the accelerator that deviate from the ideal pulse shape prevent the beam from time-of-flight bunching to the optimum pulse length on target. This may result in insufficient energy being delivered to the target in the optimal target drive time, τ_b. To examine this issue, a small sinusoidal oscillation is added to the ideal voltage pulse of Eq. (1), such that the beam is launched as a function of time with voltage

$$V_n(t) = V_d(t) + AV_o \sin(2\pi ft) \ , \qquad (18)$$

where A is the amplitude (expressed as a percentage of the value of V_O) and f is the frequency in units of Hz. For this work, the period of the oscillations are kept large with respect to the time it takes an average ion to cross the typical AK gap. This is done because the model for the diode impedance given in Eq. (2) assumes a slowly varying dependence on voltage. For a gap of 1 cm and typical ion velocities around

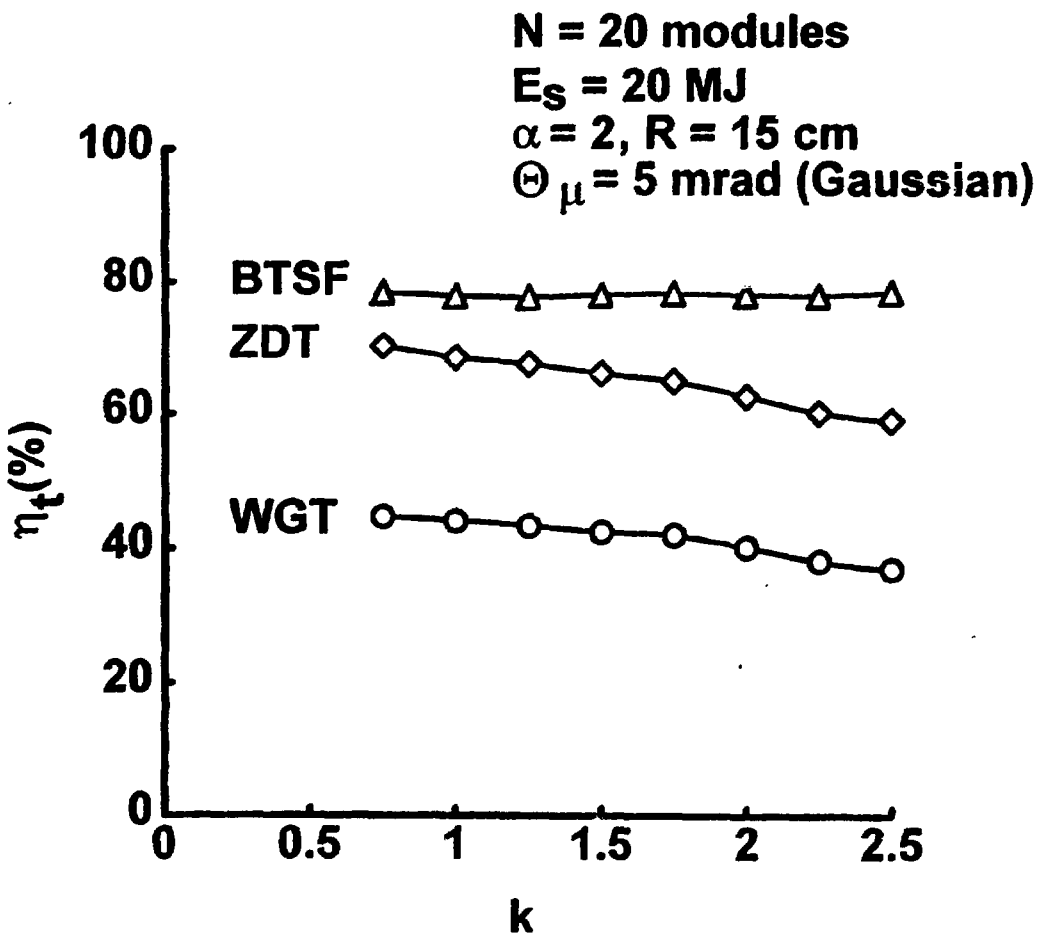

Fig. 20- Plot of η_t vs. k for R = 15 cm. Individual curves are for BTSF, ZDT, and WGT.

$v_o = (2eZ_d V_o/m_i)^{1/2} \approx 2.87 \times 10^9$ cm/s, an ion crosses the AK gap in about 1/3 ns. Therefore, only voltage oscillation periods greater than a few ns will be considered here.

Two cases of non-ideal power pulses are considered: (1) the ideal current in the diode is used with the non-ideal voltage waveform [Eqs. (2) and (18) respectively], and (2) both the current and voltage are given a non-ideal shape [Eq. (18) and Eq. (2) with $V_d(t)$ replaced by $V_n(t)$ from Eq. (18)]. For purposes of comparison, the total energy in the non-ideal pulse is normalized to the total energy in the ideal case by scaling the magnitude of the current of the non-ideal to the ideal case. The ratio, γ, of the energy in the ideal to the non-ideal system,

$$\gamma = \left(\int_o^{\tau_d} V_d(t) I_d(t) dt \right) / \left(\int_o^{\tau_d} V_n(t) I_{do} \left[\frac{V_{d,n}(t)}{V_o} \right]^k dt \right), \tag{19}$$

is multiplied by I_{do} giving the current for the non-ideal cases as

$$I_n(t) = I_{no} \left(\frac{V_{d,n}(t)}{V_o} \right)^k, \tag{20}$$

where $I_{no} = \gamma\, I_{do}$. V_d is used in Eq. (20) for case (1) and V_n is used for case (2). The current scaling is minimal ($0.98 < \gamma < 1.02$) for all cases considered here.

Oscillations of the initial voltage pulse were applied to all three transport schemes for the specific parameters of R = 15 cm, $\alpha = 2$, $k = 2$, V_{tune} = 30 MV, N = 20 modules, and Θ_μ = 5 mrad (Gaussian). Calculations were performed for $1/f$ = 10 ns over a range from $A = 0$ to $A = 0.10$. Two energy transport efficiency numbers were calculated for each run. The first, η_t, is the total energy transport efficiency defined in Section I, calculated over the entire power pulse delivered to the target, and η_t^{15} denotes the energy transport efficiency delivered to the target in the 15 ns centered at the middle of the delivered power pulse. For each transport scheme, η_t and η_t^{15} are plotted against the

range of A, illustrating the impact of non-ideal bunching that is induced from variations in the power pulse. For the BTSF case, an additional investigation into the role of the frequency, f, is analyzed for a given A.

Considering non-ideal waveforms for BTSF, given in Fig. 21, amplitudes $\geq$ 2 % can have a noticeable effect on the energy delivered in the middle 15 ns of the pulse. The combined effect of altered bending in the diode from Eq. (8) (with V_d replaced by V_n), coupled with non-ideal time-of-flight pulse compression, results in additional energy transport losses for $A \geq$ 2 % and $1/f$ = 10 ns. η_t^{15} at A = 2 % is 70 %, an 8 % drop from the ideal waveform calculation, and continues to fall off as A increases. The solid markers in Fig. 21 (and Figs. 23, 24) at A = 5 % indicate data points for case (2), while the open data points are for case (1) described above. It is can be concluded that the non-ideal voltage waveform drives a temporal spreading of the pulse that reduces η_t^{15}. Small fluctuations in voltage and current do not significantly reduce η_t^{15} by defocusing the beam. Over the range A = 0 to 7 %, η_t was essentially constant at 78 % , but falls slightly at A = 10 %, to an η_t of 75 %.

Also for BTSF, the role of the frequency of the oscillations in the reduction in η_t was investigated by varying $1/f$ over the range of 5 to 30 ns for A at ±5 %. Figures 22 and 23 show only a small variation in η_t while large variations in η_t^{15} are observed. In Fig. 22, a small deviation in η_t of ±2 % around the value for the ideal pulse is observed for $1/f < 20$ ns. For larger $1/f$, the deviation in η_t from the ideal pulse begins to increase because the frequency of oscillation is low enough to dominate the waveform characteristics. For example, when $1/f$ = 30 ns, exactly one sinusoidal oscillation occurs over the pulse time. The systematic variation seen in Fig. 23 (and to a lesser extent in Fig. 22) results from this dominant effect on the ideal waveforms when the full pulse, $2\pi f\tau_d$, is close to multiples of 2π. When the frequency of the oscillations becomes high enough and many oscillations occur within τ_d, this effect begins to smear out and an average reduction in η_t^{15} is observed, resulting in an 8 % drop in η_t^{15} for $1/f < 10$ ns. In

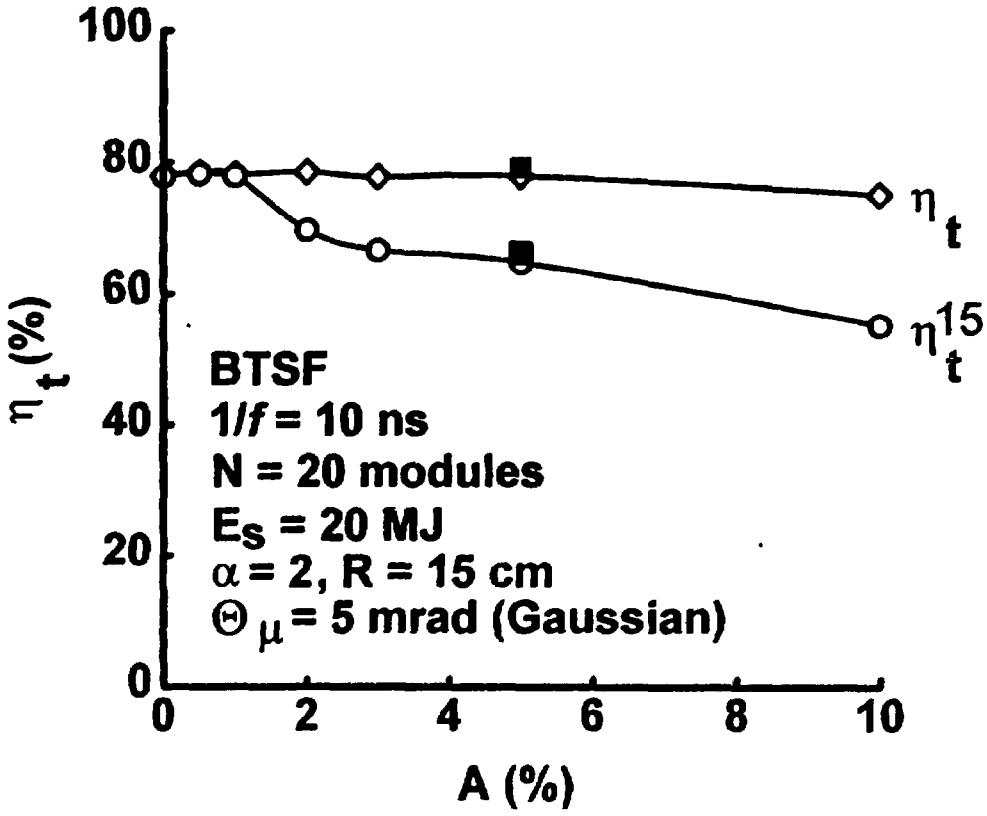

Fig. 21 - Plot of η_t vs. A for BTSF for non-ideally bunched wave forms with R = 15 cm and $1/f$ = 10 ns. Individual curves are for η_t (total energy efficiency on target, full pulse) and η_t^{15} (energy efficiency on target in the middle 15 ns of the pulse). Hollow data points represent calculations for case (1) (non-ideal voltage) and solid data points represent calculations for case (2) (non-ideal voltage and current) as discussed in the text. For these cases $V_{tune} = V_o$.

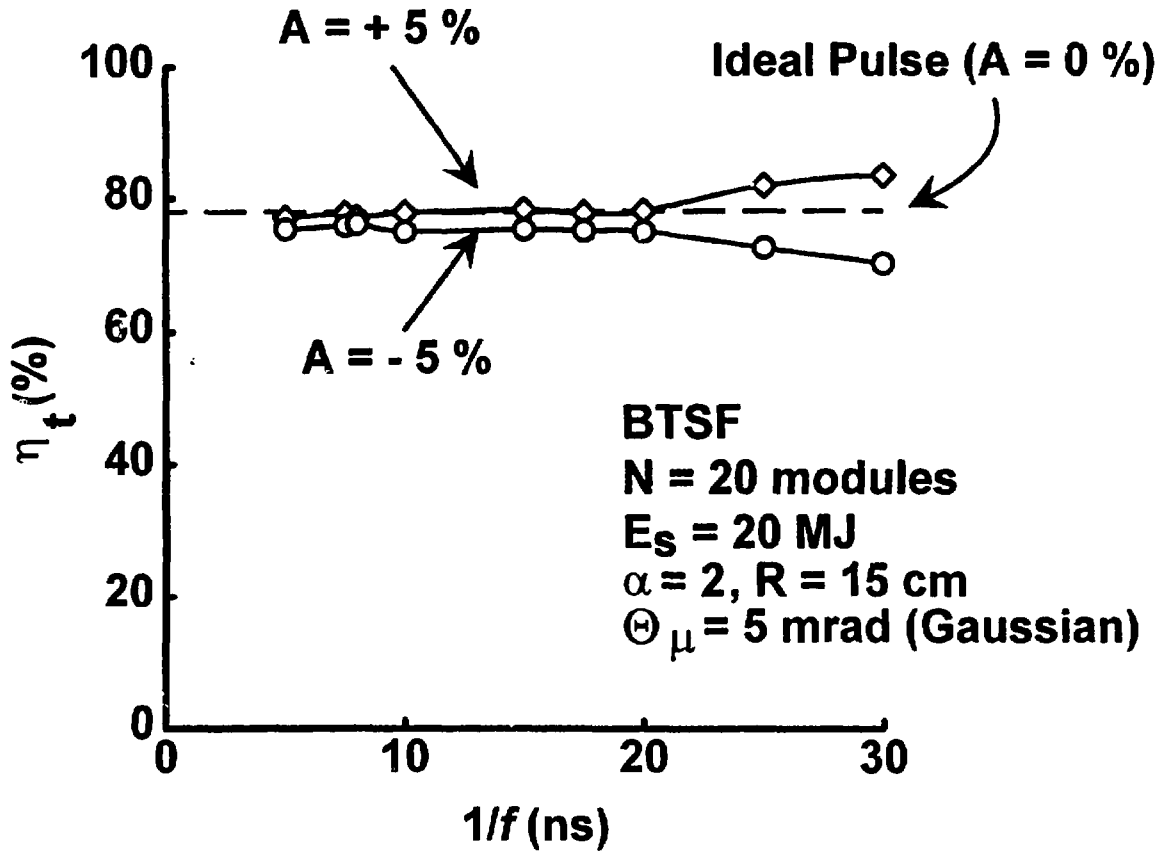

Fig. 22- Plot of η_t vs. $1/f$ for BTSF for non-ideally bunched wave forms with R = 15 cm. Individual curves are for A = 0 % (ideal pulse), +5 %, and -5 %. For these cases $V_{tune} = V_o$.

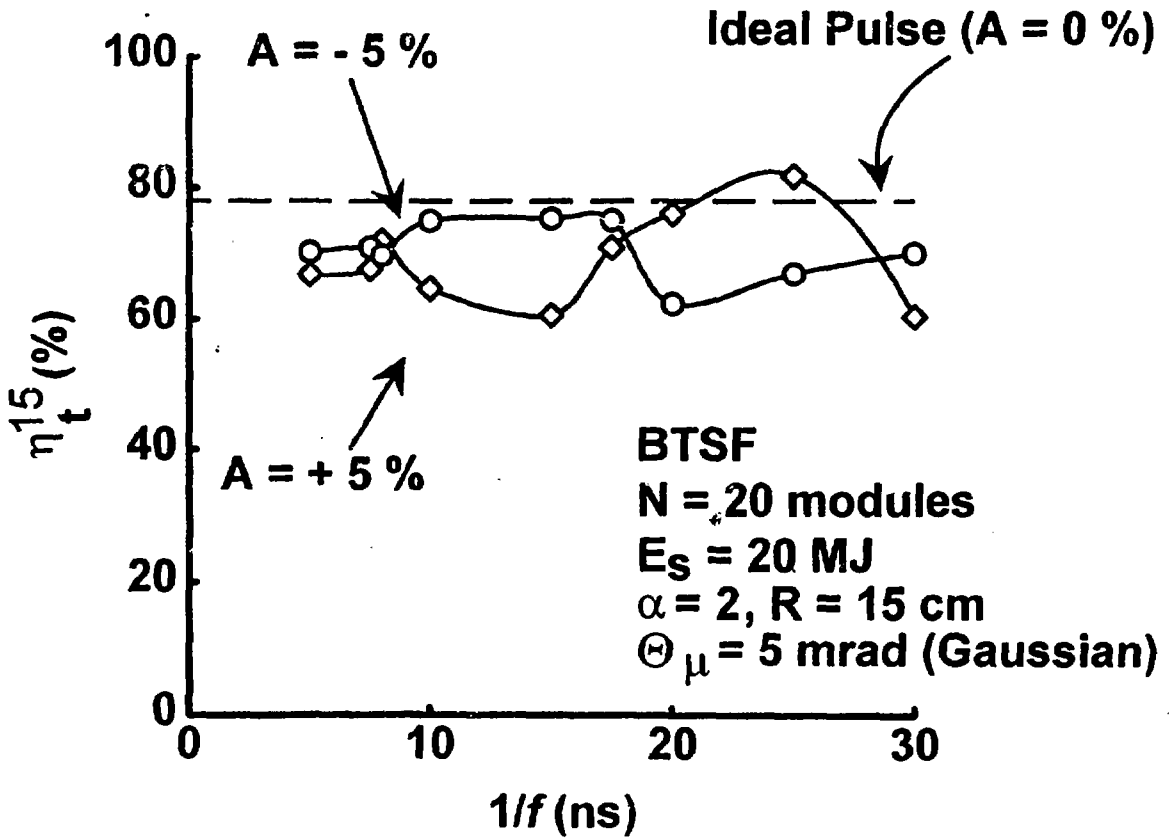

Fig. 23 - Plot of η_t^{15} vs. $1/f$ for BTSF for non-ideally bunched wave forms with R = 15 cm. Individual curves are for A = 0 % (ideal pulse), +5 %, and -5 %. For these cases $V_{tune} = V_o$.

Fig. 23, the curves for $+A$ and $-A$ are almost symmetric with respect to each other but on average are about 8 % below that of the ideal case ($A = 0$).

For ZDT and WGT, calculations similar to the BTSF case were made, fixing $1/f$ at 10 ns and varying A from 0 to 10 %. Results for these calculations are shown in Figs. 24 (ZDT) and 25 (WGT). Both plots show a trend almost identical to the BTSF case, where significant discrepancies between η_t and η_t^{15} begin at $A = 2$ %. As for the BTSF case, the hollow data points in Figs. 24 and 25 indicate calculations for case (1) and solid data points represent calculations for case (2). For ZDT in Fig. 24, η_t is 63 % on average. At $A = 2$ %, η_t^{15} is 57 %, a drop of 6 % from the ideal case. As A increases, η_t^{15} continues to drop off almost linearly with $\eta_t^{15} = 44$ % at $A = 10$ %. For WGT in Fig. 25, η_t is 40 % on average. Again, at $A = 2$ %, η_t^{15} is 36 %, a drop of only 4 % from the ideal case. As A increases, η_t^{15} continues to drop off almost linearly with $\eta_t^{15} = 28$ % at $A = 10$ %. These results again point to variations in the voltage pulse driving the non-ideal bunching, resulting in a reduction in η_t^{15}. The larger the amplitude of the disturbance, the longer the final pulse duration will be.

V. Summary And Conclusions

In this paper, transported power and energy efficiency studies have been carried for parameters relevant to the design of a light-ion LMF. The square microdivergence profile used in previous studies[5,6,7,9] has been replaced with a Gaussian profile that has a half-width, half-maximum $\Theta_\mu = 5$ mrad. Losses in η_t of 25 % or less result primarily from ions being in the "wings" of the distribution. A comparison of η_t between square and Gaussian microdivergence profiles over a range of R is presented in Section II for the BTSF, ZDT, and WGT schemes. Results are shown in Figs. 6, 7, and 8. For the Gaussian microdivergence cases shown, η_t is reduced from the square microdivergence case by less than 12 % for BTSF, 9 % for ZDT, and 20 % for WGT. The reduction for

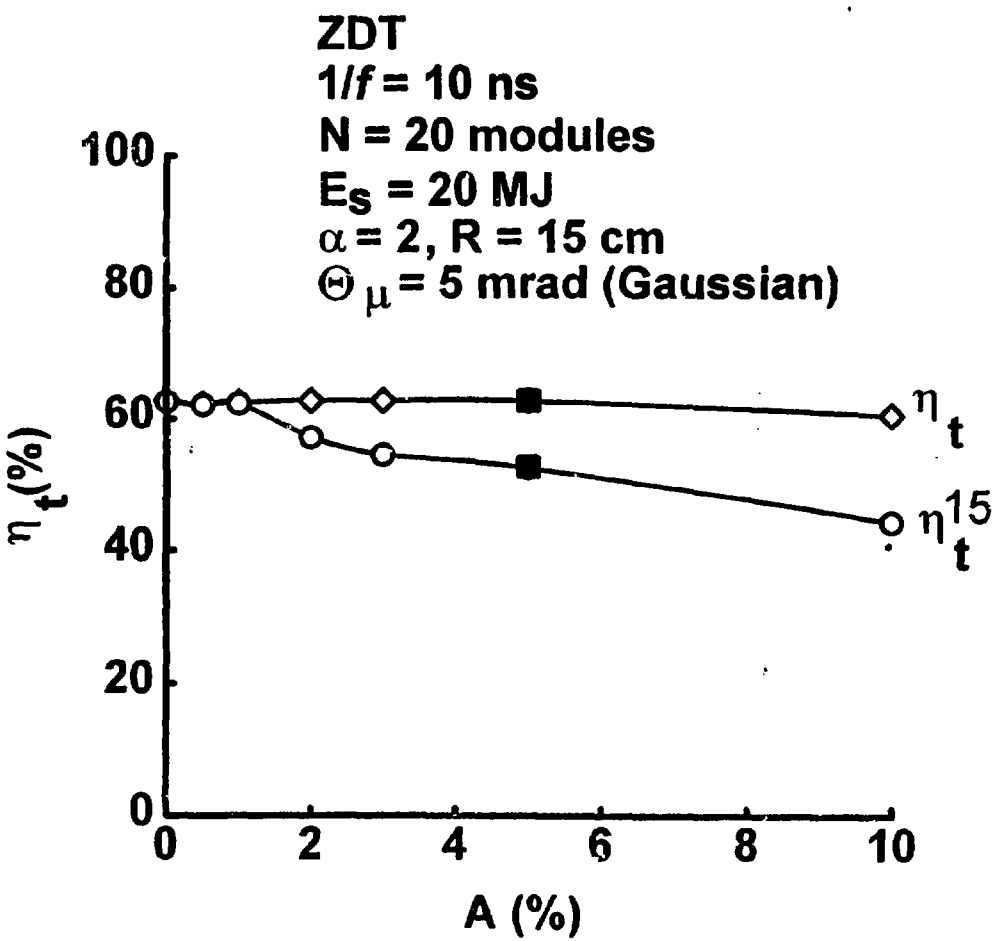

Fig. 24- Plot of η_t vs. A for ZDT for non-ideally bunched wave forms with R = 15 cm and $1/f$ = 10 ns. Individual curves are for η_t (total energy efficiency on target, full pulse) and η_t^{15} (energy efficiency on target in the middle 15 ns of the pulse). Hollow data points represent calculations for case (1) (non-ideal voltage) and solid data points represent calculations for case (2) (non-ideal voltage and current) as discussed in the text. For these cases $V_{tune} = V_o$.

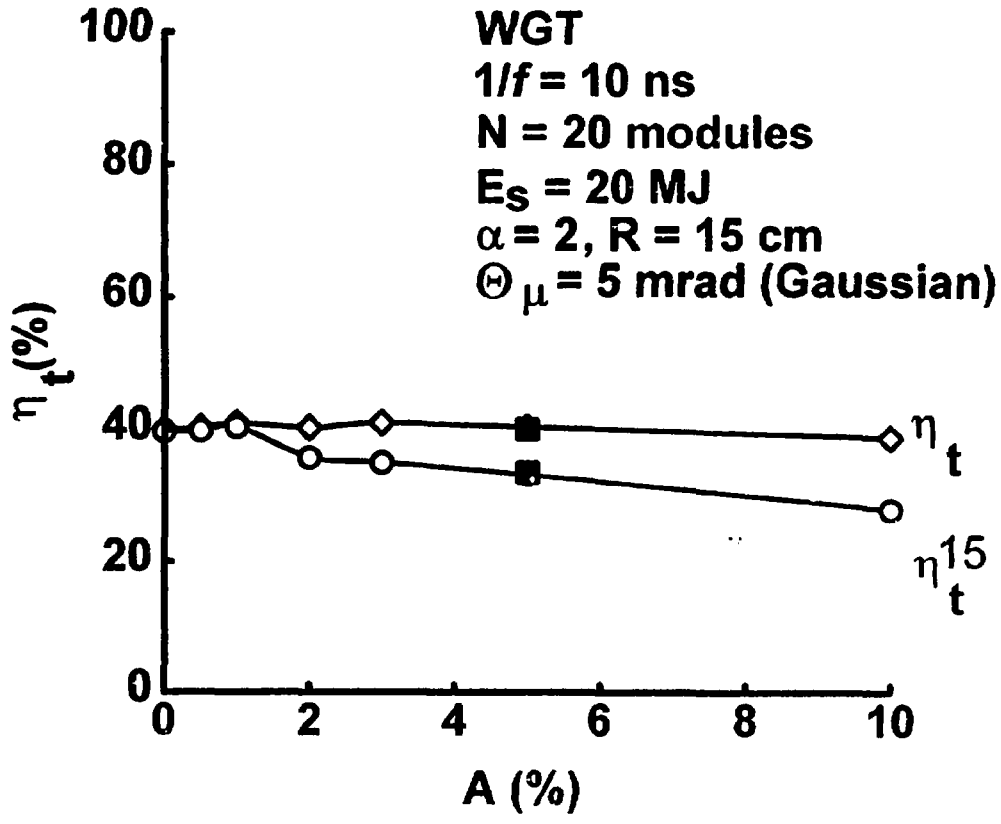

Fig. 25 - Plot of η_t vs. A for WGT for non-ideally bunched wave forms with R = 15 cm and $1/f$ = 10 ns. Individual curves are for η_t (total energy efficiency on target, full pulse) and η_t^{15} (energy efficiency on target in the middle 15 ns of the pulse). Hollow data points represent calculations for case (1) (non-ideal voltage) and solid data points represent calculations for case (2) (non-ideal voltage and current) as discussed in the text. For these cases $V_{tune} = V_o$.

WGT is the largest because the forward peaked Gaussian distribution produces more low-angular-momentum ions that strike the guide wire and are removed from the beam. The reduction for BTSF is minimized because the spot size $F\Theta_\mu$ is smaller that the target radius.

The impact of power efficiency tuning on η_t has been examined for the BTSF, ZDT, and WGT transport schemes for a range of parameters that are applicable to the design of a light-ion LMF system. Results indicate that moving the point of peak power efficiency to three-quarters of the pulse time results in maintaining a near optimal value for η_t while achieving high Γ_t^{end} at the end of the pulse. For the BTSF baseline case at $R = 15$ cm, tuning the power pulse to maximize Γ_t at three-quarters of the pulse time yields a Γ_t^{end} of 89 % with an η_t of 73 %. This means that only 6 % of overall energy is sacrificed to gain 14 % of instantaneous power at the tail of pulse. By tuning to the end of the pulse, only 1 % more instantaneous power can be obtained at the expense of an additional 17 % of energy loss. Therefore tuning to the achieve instantaneous power at the three-quarters point in the power pulse yields the optimum performance for this system. This overall conclusion is the same for the ZDT and WGT systems.

In addition, the diode impedance model has been systematically varied in order to examine the impact of current scaling with voltage on η_t. The value of the scaling constant, k, was varied over a range of values that may result from advanced applied-B diode design, including two-stage diodes. Because BTSF is an achromatic system, virtually no variation in η_t was found for values of k in the range of 0.75 to 2.5, even though higher values of k result in larger manifestations of the focus sweep effect.[9] It was assumed that the achromatic matching constraint placed on Δ can be met even when Δ becomes large as k approaches 0.5. For the ZDT and WGT schemes, some variation in η_t was found, with η_t becoming larger as k decreases. This results primarily from the increasing focus sweep effect as k increases for these nonachromatic systems. These

calculations were performed for one point design in the LMF parameter regime, namely $R = 15$ cm, $N = 20$ modules, $\alpha = 2$, $E_s = 20$ MJ, $F = 150$ cm, $V_{tune} = V_o$, and $\Theta_\mu = 5$ mrad.

Deviations from the ideal form of the voltage in a programmed power pulse can lead to temporal spreading of the bunched pulse at the target. The effect of non-ideal waveforms on η_t is evaluated by adding a sinusoidally variation to the ideal voltage and current pulses produced at the diode. Results indicate that sinusoidal oscillations with an inverse frequency, $1/f$, of 10 ns and amplitudes greater than 2 % of the average voltage, V_o, reduces η_t delivered to the target in the optimal bunched pulse length, τ_b, denoted as η_t^{15}. For BTSF, this results in an 8 % drop in η_t^{15}, as shown in Fig. 21. As the amplitude of the oscillation is increased, the spread in the pulse increases, further reducing η_t^{15}. For ZDT and WGT, similar results are obtained, as shown in Figs. 24 and 25, respectively. However, Fig. 23 demonstrates that results do depend on the frequency and sign of the amplitude. The results quoted above are close to "worst-case" numbers. Because defocusing does not occur, the ideal pulse efficiency is also recovered if longer pulse durations are acceptable.

This work extends a previous investigation into LMF transport point designs,[9] examining the impact of the focus sweep effect on transport efficiency. Further issues that need to be considered in order to accurately determine η_t for specific designs include ion-beam species purity, waveform efficiency, and beam energy losses during transport. Details of the ion beam source model, including the radial dependence of Δ and an accurate microdivergence model must be improved in order to further quantify η_t.

VI. Acknowledgments

This work was supported by US DOE through Sandia National Laboratories.

VII. References

1. J.J. Ramirez, R.W. Stinnett, D.L. Johnson, C.L. Olson, T.A. Mehlhorn, J.T. Crow, J.P. Quintenz, K.R. Prestwich, M.P. Desjarlais, R.E. Olson, G.O. Allshouse, T.H. Martin, J.P. VanDevender, D.L. Cook, S.A. Slutz, K.B. Coachman, T.R. Lockner, B.N. Turman, S.A. Goldstein, J.N. Olsen, R.R. Peterson, and R.L. Engelstad, Fusion Tech. **15**, 350 (1989).
2. J.J. Ramirez, D.L. Cook, J.K. Rice, M.K. Matzen, D.L. Johnson, J.D. Boyes, C.L. Olson, K.R. Prestwich, M.J. Clauser, T.A. Mehlhorn, R.W. Stinnett, G.O. Allshouse, G.L. Kulcinski, G.A. Moses, R.R. Peterson, and R.L. Engelstad, Laser and Part. Beams **11**, 423 (1993).
3. C.L. Olson, in the Proceedings of the 1989 Particle Accelerator Conference, F. Bennett and J. Kapta, eds. (Chicago, Il, March 20-23, 1989), p. 1011.
4. D. Mosher, D.D. Hinshelwood, J.M. Neri, P.F. Ottinger, J.J. Watrous, C.L. Olson, and T.A. Mehlhorn, in the Proceedings of the 8th International Conference on High-Power Particle Beams, B.N. Breizman and B.A. Knyazev, eds. (Novosibirsk, USSR, July 2-5, 1990), p. 26.
5. P.F. Ottinger, D.V. Rose, J.M. Neri, and C.L. Olson, J. Appl. Phys. **72**, 395 (1992).
6. P.F. Ottinger, D.V. Rose, D. Mosher, and J.M. Neri, J. Appl. Phys. **70**, 5292 (1991).
7. J.J. Watrous, D. Mosher, J.M. Neri, P.F. Ottinger, C.L. Olson, J.T. Crow, and R.R. Peterson, J. Appl. Phys. **69**, 639 (1991).
8. R.F. Hubbard, M. Lampe, G. Joyce, S.P. Slinker, I. Haber, and R.F. Fernsler, Part. Accel. **37-38**, 161 (1992).
9. P.F. Ottinger, D.V. Rose, and C.L. Olson, J. Appl. Phys. **75**, 4402 (1994).

10. R.E. Olson, G.O. Allshouse, D.L. Cook, T.R. Lockner, M.G. Mazarakis, C.L. Olson, D.L. Smith, in the Proceedings of the 15th IEEE Symp. on Fusion Engineering (Hyannis, MA, October 11-15, 1993), to be published.

11. J.P. Quintenz and D.B. Seidel, Sandia Nat. Lab. Report SAND84-1336 (June 1984).

12. S.A. Slutz, and M.P. Desjarlais, J. Appl. Phys. 67, 6705 (1990).

VIII. List Of Variables

η_t	Energy transport efficiency
η_t^{15}	Energy transport efficiency for the middle 15 ns of the power pulse
V_o	Average diode voltage
Z_d	Beam charge state in the diode
Z_t	Beam charge state after stripping
E_t	Energy on target
E_s	Energy of the system
α	Bunching factor
N	Number of modules
τ_d	beam pulse duration in the diode
τ_b	beam pulse duration at target
I_{do}	Ion current in the diode at time when $V_d(t) = V_o$
I_{no}	Ion current in the diode at time when $V_d(t) = V_o$ for case (2) in text ($V_n(t)$ is a function of V_d and t)
I_{to}	Average ion current at the target
R	Diode outer radius
R_i	Diode inner radius
$V_d(t)$	Voltage wave form at the diode
$V_n(t)$	Non-ideal voltage wave form at the diode
$V_t(t)$	Voltage wave form at the target
V_{tune}	Tuning voltage
Δ	Diode vacuum gap spacing
c	Speed of light
e	Electron charge
m_i	Beam ion mass
F	Focal distance
D	Total transport distance
L	Transport distance (~ 250 cm)
k	Ion current scaling constant
T	Arrival time of beam front on target
f	Frequency of non-ideal pulse oscillations
γ	Energy correction factor
$I_d(t)$	Beam current at the diode
$I_n(t)$	Beam current at the diode, non-ideal wave form case
$I_t(t)$	Beam current at the target
Θ_μ	Microdivergence
Γ_t	Instantaneous power efficiency on target
Γ_t^{tune}	Instantaneous power efficiency on target at the tuning time
Γ_t^{end}	Instantaneous power efficiency on target at end of pulse
$\Theta_a(r)$	Anode surface shaping function in the diode

$\Theta_b(r, t)$	Self-magnetic bending angle function for beam at diode
$\Theta_s(r, t)$	Beam steering function at diode
Θ_0	Steering angle coefficient
$v_d(0)$	Ion velocity at beginning of beam pulse
R_s	Solenoid inner radius
L_s	Solenoid axial length
r_a	Transport channel entrance aperture radius
r_c	Discharge channel radius
r_w	Wire radius
ω_c	Ion cyclotron frequency
I_c	Discharge channel current
I_w	Central guide wire current
d	Standoff distance
r_t	Target radius